Investigating rates and mechanisms of lateral erosion in a small bedrock river using erosion pins, structure-from-motion photogrammetry, and optically stimulated luminescence dating: Konza Prairie, northeast Kansas

by

Abbey Leigh Marcotte

B.S., Kansas State University, 2017

A THESIS

submitted in partial fulfillment of the requirements for the degree

MASTER OF ARTS

Department of Geography and Geospatial Sciences
College of Arts and Sciences

KANSAS STATE UNIVERSITY
Manhattan, Kansas

2020

Approved by:

Major Professor
Dr. Abigail L. Langston

Copyright

Abstract

Bedrock rivers play a critical role in landscape evolution by leaving signatures of past climate shifts, base level changes, and tectonic uplift in the landscape. While much is known about the mechanics of vertical bedrock incision, the fluvial processes driving lateral bedrock erosion and the timescales over which it occurs remain poorly understood. In order to advance our understanding of how bedrock rivers erode laterally over time, I investigated past and present erosion rates at Kings Creek, an incised stream in northeast Kansas, U.S.A. This system consists of horizontally bedded alternating layers of limestone and shale, presenting a unique setting to study rates and mechanisms of lateral bedrock erosion. Erosion pins and structure from motion (SfM) were used to determine annual lateral erosion rates and spatio-temporal patterns of erosion along bedrock channel banks. Single-grain optically stimulated luminescence (OSL) dating of fluvial deposits overlying a strath terrace was used to determine the depositional age of fluvial deposits and infer the duration of lateral channel mobility during terrace occupation.

Lateral erosion rates of limestone measured during this study averaged 20.82 mm/yr and shale lateral erosion rates range from 38.81 – 53.41 mm/yr. Field observations indicate that plucking is the dominant erosion mechanism in both lithologies. These modern lateral bedrock erosion rates are much higher than originally anticipated owing to several high magnitude flow events during an exceptionally wet year. The OSL ages of fluvial deposits sourced from the strath terrace suggest that Kings Creek experienced periods of aggradation, incision, and channel migration during the late Pleistocene. Together, the annual erosion rates and OSL ages provide information about rates of lateral erosion and paleochannel mobility, thus improving our understanding of the timing and processes linked to how bedrock rivers erode laterally to form wide bedrock valleys.

Table of Contents

List of Figures

List of Tables

Acknowledgements

I would like to first acknowledge my advisor, Dr. Abigail Langston, and my committee members, Dr. Arnaud Temme, Dr. Shawn Hutchinson, and Dr. Kendra McLauchlan, for their contributions and guidance throughout this project. Abby was an outstanding mentor, with endless patience and encouragement. I could not have made it through these two years without her enthusiasm and support through the ups and downs. This research was possible with funding from the Geological Society of America, Kansas State University Department of Geography & Geospatial Sciences, and the Kansas Association of Mappers.

Many thanks go to our Geomorphology Group – Nathan Brownstein, Colleen Gura, Nicholas McCarroll, Michael Stumpff, Jordan Watson, and our fearless leaders Abby and Arnaud – for their scientific enthusiasm, advice, and challenges. Special thanks to Michael Stumpff for always (sometimes reluctantly) helping me with my field work at Konza.

I thank Amanda Keen-Zebert and Christina Neudorf from the Desert Research Institute in Reno, NV for allowing me to work in the luminescence lab, training me OSL dating techniques, and providing advice while I was analyzing my OSL data. I am also grateful to the Soil Geography and Landscape Group at Wageningen University for allowing me to follow the 4th Dimension in Earth's Surface course, and to the Stoorvogel family (my 'Dutch family') for welcoming me into their home during my stay in the Netherlands.

Finally, my most heartfelt thanks to my dear family and friends for supporting my academic and research endeavors, no matter how crazy they may seem at first. And providing me the occasional free meal. I am especially grateful for their encouragement and for reminding me that having hobbies and an identity outside of being a student is important, too.

Dedication

To my grandfather, John K. Strickler. A champion of nature, my biggest cheerleader, and the reason I do what I do. I wish you were here to see this.

.

Chapter 1 - Introduction

1.1 Introduction

Bedrock rivers play a central role in landscape evolution by communicating signals of climate shifts, base level changes, and tectonics through landscapes (Hancock et al., 1998; Whipple & Tucker, 1999; Whipple, 2004). Vertical erosion and subsequent channel adjustment in bedrock systems has been a highly researched area for the past 30 years through landscape evolution models (e.g., Whipple & Tucker, 1999), flume experiments (e.g., Sklar & Dietrich, 2001), and field studies (e.g., Whipple et al., 2000). As a result, the mechanics of vertical bedrock incision, which is driven by combination of stream discharge and sediment supply and transport, are relatively well-understood. However, very little is known about the rates and mechanics of lateral bedrock erosion. This presents a fundamental knowledge gap in understanding how bedrock rivers respond to climatic and tectonic changes, and how channel geometry is maintained and changed over time. Additionally, wide bedrock valleys are indicative of significant lateral erosion. A complete understanding of the controls on lateral bedrock erosion and valley widening is necessary to interpret strath terrace formation.

Vertical erosion happens more rapidly than lateral erosion (Dühnforth et al., 2012), but the timing of shifts in how long a river spends laterally eroding versus downcutting remain unclear (Bufe et al., 2017). Strath terraces are evidence of periods of sustained lateral erosion that carves a wide bedrock valley and outpaces vertical incision. Because strath terraces are used to interpret past periods of climate change (e.g., Hancock et al., 1999), mechanisms of both vertical and lateral erosion must be considered together in order to understand flights of strath terraces. However, due to an incomplete understanding of the drivers of lateral erosion, it is difficult to interpret how climate, and fluvial processes affected by climate, influenced river erosion in the past and will continue to shape landscapes in the future.

Physical evidence for lateral erosion suggests that sediment supply encourages lateral bedrock erosion, and models also often invoke shear stress to predict lateral erosion rates (Hancock & Anderson, 2002). Enhanced lateral erosion is favored in weak lithologies (e.g., Montgomery, 2004) and high sediment supply environments shield the channel bed and drive sediment impacts on the channel banks (Fuller et al., 2016). Yet few studies suggest specific mechanisms or drivers of lateral erosion (Langston & Tucker, 2018), nor do many measure the

rate at which lateral bedrock erosion occurs in natural channels (Beer et al., 2017). Due to the insufficient understanding of these interacting processes, lateral migration in bedrock channels is neglected in nearly all existing landscape evolution models (e.g., Langston & Tucker, 2018). Furthermore, landscapes with bedrock units of variable erodibility has long been recognized as an important factor in landscape evolution, yet they are seldom systematically studied in landscape evolution models (Forte et al., 2016; Perne et al., 2017).

1.2 Objectives

The purpose of this study is to determine annual rates and mechanisms of lateral bedrock erosion, and to determine the duration of lateral channel mobility during strath terrace occupation in Kings Creek, northeast Kansas, USA. Kings Creek is a small bedrock river located within Konza Prairie and the system has alternating layers of shale and limestone, thus presenting a unique setting in which controls on lateral bedrock erosion can be further investigated. This study will provide an increased understanding of how bedrock rivers erode laterally over time through direct field measurements and observations, and luminescence dating. The following primary questions are used to guide this research:

(1) What are the annual-scale rates and mechanisms of lateral bedrock erosion? This question will be answered using erosion pins, structure-from-motion photogrammetry, and trail cameras. It focuses on the spatio-temporal patterns of bedrock erosion rates over the duration of this study at meander bends which are currently eroding into bedrock.

(2) What is the duration of lateral channel mobility during strath terrace occupation? This question will be answered using single-grain optically stimulated luminescence (OSL) dating of fluvial deposits capping a strath terrace. These depositional ages will yield an age of terrace occupation, as well as characterize deposition rates and duration of lateral channel mobility during the period of terrace occupation in this system.

Chapter 2 - Background

2.1 Primer on Bedrock Rivers

Two distinct types of rivers exist: alluvial and bedrock rivers. Alluvial channels form when the sediment supply (Qs) exceeds the sediment transport capacity of the stream (Qc). Alluvial rivers are characterized by having banks and beds that are composed of sediment, as such, these channels are prone to shifts in channel pattern and position as alluvium is eroded and deposited (Schumm, 1985). Bedrock rivers are characteristic of when transport capacity exceeds the sediment supply (Qc > Qs). Bedrock rivers have channel banks and bed that are largely comprised of in-place bedrock and may be mantled with thin, transient alluvium (e.g., Whipple et al., 2013). While often found in mountainous regions (e.g., Montgomery & Buffington, 1997), bedrock rivers are also found in other areas where the gradient is more gradual such as the Flint Hills, Ozark Plateau, or the Mid-Atlantic region in the United States. Some similarities exist between the two types of rivers. For example, bedrock rivers share aspects of hydraulic geometry with alluvial rivers, and both types of rivers have a width scaling relationship (Montgomery & Gran, 2001). However, the physical laws of channel erosion governing alluvial rivers cannot be applied to bedrock rivers because these two channel types function in fundamentally different ways, such that different equations and investigations are needed to describe their behavior and evolution.

Bedrock rivers leave signatures of past climate shifts, tectonics, and base level change through landscapes in their longitudinal profile, and in the form of fluvially carved strath terraces (Hancock et al., 1998; Whipple & Tucker, 1999; Whipple, 2004). Spatial and temporal effects of tectonic uplift are often observed in an abrupt change or slope-break in channel steepness (i.e., a knickpoint; Whipple and Tucker, 2002; Whipple et al., 2013) or flights of strath terraces (Pazzaglia, 2013). Perturbations may also be triggered by changes in the river's base level due to local or regional climate conditions, causing the channel to adjust its slope to a new sea level or local base level (i.e., Crosby and Whipple, 2006). Bedrock rivers control the local base level for adjacent hillslopes, such that the rate of hillslope erosion is controlled in part by rate of bedrock incision (e.g., Mudd & Furbish, 2007; Roering et al., 2001). These examples reveal that past changes in tectonics and climate are recorded in bedrock river landscapes, demonstrating their unique role in landscape evolution.

2.2 Mechanisms of Bedrock Erosion

Fluvial incision into bedrock is achieved largely through dissolution, abrasion, and plucking (e.g., Whipple et al., 2000). Dissolution is the chemical weathering of soluble lithologies, such as carbonates, which may also weaken the bedrock surface and make it more susceptible to abrasion and plucking (Whipple et al., 2013). Fluvial abrasion occurs when bedrock is eroded due to sediment impacts that contribute to the incremental wear of the bed. Erosion via abrasion increases with increasing amounts of sediment due to greater sediment impacts (Sklar & Dietrich, 2004; Attal & Lavé, 2009; Lamb et al., 2008). If there is as surplus in sediment, there will be a greater number of sediment impacts on the channel bed and an increase in erosion; this is known as the 'tools effect'. However, too much sediment could also lead to an increase in sediment covering and protecting the channel bed from sediment impacts, which is known as the 'cover effect' (Sklar & Dietrich, 2001; 2004).

Plucking is the removal of bedrock blocks from the channel bed. Plucking occurs when hydraulic lift forces are sufficient to extract blocks from the channel bed (Whipple et al., 2000). A variety of processes, such as freeze/thaw, weathering, bedload impacts and wedging, and crack propagation by intense turbulent flows, contribute to the fracture and loosing of joint blocks (Whipple et al., 2000). Flows capable of plucking tend to occur less frequently than flows capable of abrasion (Snyder et al., 2003), but when plucking occurs, erosion is much more efficient than via abrasion and leads to large amounts of erosion in a small amount of time such as during flood events capable of entraining and transporting large blocks (Lamb et al., 2015; Baynes et al., 2015; Lamb & Fonstad, 2010). For example, Snyder et al., (2003) observed bedrock slabs plucked from the channel bed up to 4 m long x 2 m long x 30 cm thick as a result of a flood event. Erosion mechanisms may act in concert and are controlled by lithologic factors such as rock strength and joint spacing (Whipple et al., 2000). Lithological resistance to erosion in natural settings is highly variable, which contributes to spatial variations in the mechanisms and rates of fluvial incision (e.g. Whipple et al., 2000).

Models and field studies have shown that thresholds are important for bedrock erosion in both plucking and abrasion dominated systems (Snyder et al., 2003). Thresholds influence erosion such that bedrock often only erodes if a certain discharge threshold is met, beyond which bed cover is mobilized and/or bedrock pieces are entrained and transported via plucking. These

larger discharge events may occur infrequently making vertical incision episodic rather than continuous in locations that are threshold dominated (Snyder et al., 2003; Baynes et al., 2015).

2.3 Lateral Bedrock Erosion

Despite the advances in understanding of vertical bedrock erosion, comparatively few studies have attempted to resolve controls on lateral bedrock erosion processes and rates. Recently, researchers have begun studying processes of lateral bedrock erosion and suggest that sediment (e.g., Fuller et al., 2016; Beer et al., 2017; Langston & Tucker, 2018) and bedrock lithology (e.g., Johnson & Finnegan, 2015; Langston & Temme, 2019a) largely control rates of lateral erosion. However, considerable research is needed to achieve the same level of understanding of processes and mechanisms of lateral bedrock erosion compared to vertical incision.

Sediment plays a fundamental role in both vertical and lateral bedrock erosion (e.g., Whipple et al., 2000; Sklar & Dietrich, 2001). The 'tools' and 'cover' effects were developed for vertical bedrock incision; however, their concepts can be applied to lateral bedrock erosion. The 'cover' and 'tools' effect influences distribution of erosion across bedrock channels (Whipple & Tucker, 2002; Hancock & Anderson, 2002; Turowski et al., 2008), and lateral erosion that outpaces vertical incision is achieved when aggradation of sediment covering the bed inhibits vertical incision.

Sediment laterally erodes bedrock through abrasion and sediment impacts on the channel banks. This happens along meander bends where channel curvature is highest (i.e., Wohl & Ikeda, 1998; Cook et al., 2014; Beer et al., 2017), and can also happen independently of the sediment cover effect. Sediment may also play a role in lateral erosion of bedrock walls when larger roughness elements in the channel deflect sediment towards the walls (Fuller et al., 2016).

A high sediment supply environment encourages channel mobility, thus driving lateral erosion and the development of wide bedrock valleys (Tomkin et al., 2003; Wickert at al., 2013; Langston & Tucker, 2018; Bufe et al., 2016). Greater channel mobility as a result of high sediment load contributes to lateral erosion due to a higher frequency of contact between the river and channel banks (Bufe et al., 2016; Wickert at al., 2013).

Lateral erosion rates are often greatest in weak lithologies, such as mudstones or sandstone (Montgomery, 2004; Johnson & Finnegan, 2015; Collins et al., 2016). Rapid lateral erosion of weak lithologies often happens via plucking (Langston & Temme, 2019b), yet

plucking has been noted as the dominant erosion mechanism even in massive or resistant lithologies, such as quartzite when the resistant lithology is highly fractured (Spotila et al., 2015). Mudstones may erode more rapidly even when not submerged due to cyclical wetting and drying cycles that decrease the tensile strength and cause crumbling upon drying (Montgomery, 2004), and can be easily swept away by the flow (Johnson & Finnegan, 2015). Additionally, rapid weathering of weak lithologies promotes development of a wide beveled bedrock valley that could become a fluvial strath terrace once abandoned (Montgomery, 2004; Johnson & Finnegan, 2015; Schanz & Montgomery, 2016).

2.4 Measuring Modern Lateral Erosion

A range of field techniques exist for measurements of lateral bank erosion through space and time such as repeat cross section measuring, erosion pins, and repeat photogrammetric surveys (Lawler, 1993 and references therein). Each technique has its advantages and limitations regarding data resolution and time scale of interest that should be taken into consideration before selection.

2.4.1 Erosion Pins

In bedrock river settings, erosion pins are used to measure vertical bed incision and lateral erosion rates (e.g., Collins et al., 2016; Stock et al., 2005). The erosion pin technique is a widely used method to study process rates and mechanism of bank erosion (e.g., Lawler, 1993; Hooke, 1979; Couper & Maddock, 2001; Collins et al., 2016) due to its simplicity in installation and measurement and affordability. The technique is usually employed for short timescale studies spanning from days or months to a few years. The data resolution is fine scale, with the ability to detect small amounts of bank erosion (order of mm) and data be obtained at relatively frequent intervals.

2.4.2 Structure from Motion Photogrammetry

Structure from motion (SfM) is a relatively low-cost photogrammetric technique that creates high resolution three-dimensional surfaces, such as digital elevation models (DEM) or point clouds, from a series of multiple overlapping images. SfM has emerged in the last decade as a powerful tool for geoscientists, as capturing datasets in a range of complex landscapes is now feasible (i.e., Westoby et al., 2012). SfM has been used to study bank erosion and deposition patterns (Prosdocimi et al., 2015; Duró et al., 2018; Jugie et al., 2018;), sediment transport

(Marteau et al., 2017), and channel morphology (Javernick et al., 2014; Dietrich, 2016) in alluvial rivers, and to identify topographic changes in a bedrock river gorge (Cook, 2017). Resolution of the output DEM or point cloud differs from study to study depending on data acquisition and image processing, but can range from ~3 cm to 0.5 m (Rusnák et al., 2018 and references therein).

2.5 Fluvial Terraces

Rivers often leave their erosional signature on landscapes in the form of strath or fill fluvial terraces (Figure 2.1). These features represent a prolonged period of primarily lateral erosion and widening, followed by rapid vertical incision in response to shifts in climate, discharge, sediment flux, or base level (Pazzaglia, 2013; Dühnforth et al., 2012; Foster et al., 2017). Specifically, flights strath terraces are records of sustained lateral bedrock erosion and valley widening that occurred in the past. Strath terraces are flat bedrock surfaces capped with fluvial sediment ~1 – 10 m thick (Figure 2.1B). Lateral bedrock erosion that outpaces vertical erosion contributes to the widening a channel's valley and beveling of the underlying bedrock surface (e.g., Montgomery, 2004). Following a change in boundary conditions, the beveled bedrock floodplain is abandoned via incision when vertical erosion outpaces lateral erosion (Hancock & Anderson, 2002; Montgomery, 2004; Johnson & Finnegan, 2015;). Strath terrace

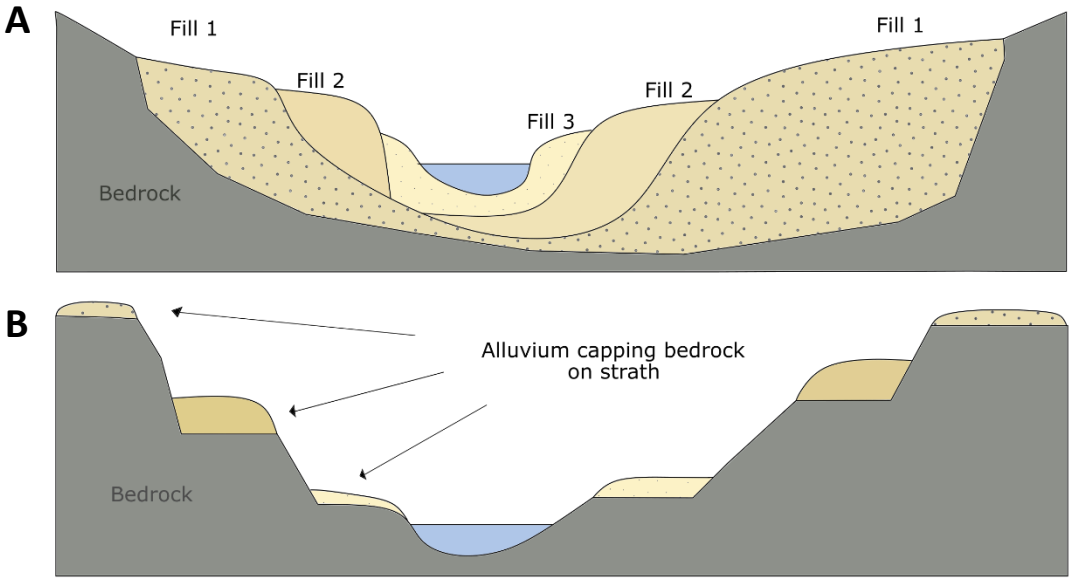

Figure 2.1 (A) Example of a sequence of fill terraces, with thick alluvial deposits filling the valley; (B) Example of flights of strath terraces cut into bedrock from different beveling and incisional periods, with alluvium of different thickness capping the flat bedrock surfaces. (*After Burbank & Anderson, 2011*).

formation may be induced by changes in sediment to water balance (e.g., Hancock & Anderson, 2002; Bufe et al., 2017), channel mobility (Bufe et al., 2016; Wickert at al., 2013), autogenic strath terrace development in meandering rivers (e.g., Crosby & Whipple, 2006; Finnegan & Dietrich, 2011), base level changes (e.g., Merritts et al., 1994), or climate shifts (e.g., Hancock et al., 1999). The most well-developed strath terraces exist primarily in channel reaches with less resistant lithologies (Collins et al., 2016; Langston et al., 2015; Montgomery, 2004; Schanz & Montgomery, 2016); however, strath terraces can also form in stronger lithologies, such as granites and quartzite (Burbank et al., 1996).

Strath terraces are created by either tectonics or climate-induced changes in sediment supply and stream discharge, such as glacial and interglacial shifts during the Pleistocene (Pazzaglia et al., 2013). Molnar et al., (1994) suggests that strath terraces in Tien Shan, China were formed and subsequently abandoned during the last glacial period. Conversely, DeVecchio et al., (2012) found strath terrace formation and aggradational events in the Western Transverse Ranges, California during the dry and warm climate of an interglacial period. Strath terraces can also form during deglacial transitions (Pan et al., 2003). These contrasting time periods of strath terrace formation suggest that development depends on the proximity of the terraces to glaciated areas and the effects the shifting climate has on strath creation. Additionally, strath terraces can develop independently of external climate and tectonic forcings (Bull, 1990; Finnegan & Dietrich, 2011) and therefore, the link between strath terrace formation and climate is not always straightforward (Foster et al., 2017).

Dating of strath surfaces or terrace alluvium has been used primarily to calculate long-term vertical bedrock incision rates (Hancock et al., 1999; Brocard et al., 2003). More recent studies date strath alluvium to determine the duration of lateral channel mobility and time spent widening the river valley (Bufe et al., 2017; Schanz & Montgomery, 2016). Common relative and absolute dating techniques utilized to date strath terraces include tephrochronology, cosmogenic radionuclide dating (e.g., Dühnforth et al., 2012), radiocarbon dating (e.g., Meyer et al., 1995; Wegman & Pazzaglia, 2002), and OSL dating (e.g., Rittenour, 2008; Keen-Zebert et al., 2013; Bufe et al., 2017). Each technique presents advantages and disadvantages, and the materials and environmental conditions should be considered before selecting a dating method (Pazzaglia, 2013).

OSL is a commonly used technique determine the depositional ages of terrace alluvium due to the near ubiquity of quartz and felspar minerals found in fluvial deposits (e.g., Summa-Nelson & Rittenour, 2012; Duller, 2004; Rittenour, 2008; Keen-Zebert et al., 2013). OSL allows fluvial material to be directly dated, and thus provides valuable age control ranging from 0 to 100 ky for quartz and up to ~300 ky for feldspar. This large age range makes it possible to reconstruct fluvial response to glacial-interglacial driven climate changes (Rittenour, 2008).

2.6 Principles of Optically Stimulated Luminescence Dating

Optically stimulated luminescence (OSL) is a Quaternary dating technique that estimates the time since quartz and feldspar minerals were last exposed to sunlight (Rhodes, 2011). Since the late 1990s, quartz has been frequently used in luminescence dating due to its near ubiquity on Earth's surface (e.g., Murray & Olley, 2002). The technique works on the principle that the materials are naturally radioactive, which causes electrons to be trapped in the crystal lattice ('hole traps') of the mineral when sediment grains are buried. The trapped electrons can be released under simulation by heat or light. The trapped electrons can be removed by sunlight exposure, such as during transport, and the sediment becomes "bleached," meaning that the electrons stored in the crystal lattice are released, and the luminescence signal is reset (Figure 2.2A). After sediment is deposited and shielded from sunlight, the luminescence signal in the grains begins to accumulate in the crystal lattice because the grains receive radiation from surrounding sediments and store part of the energy (Figure 2.2B). Under stimulation by light in the lab, the trapped energy releases photons of light—the luminescence signal (Figure 2.2C). The intensity of the luminescence signal is proportional to the burial time because the sample receives more radiation with more time; this measured luminescence signal also this is also called the equivalent dose (D_e) (Duller, 2011; Walker, 2005). The age of a sample is then determined by dividing the equivalent dose (D_e) measured in the lab by the environmental dose rate measured from geochemistry of the surrounding sediments (Duller, 2011).

Luminescence dating was first developed for multi-grain aliquots, where each aliquot may contain ~20 – 2000 grains depending on the size of grains and how the grains were mounted onto measuring discs (Roberts et al., 1999; Duller, 2008). The multi-grain method is appropriate in settings where sediment is likely fully bleached prior to burial, such as sand dunes (e.g., Kasse et al., 2007). Advances in OSL dating include the ability to date single grains of quartz or feldspar, called single-grain dating (Roberts et al., 1999). Single-grain OSL dating makes it

possible to determine if all grains in a sample share the same age (Duller, 2004). Dating of one single grain is advantageous in fluvial settings where all grains may not be exposed to daylight long enough to reset their signal – called incomplete bleaching or heterogenous bleaching – as a result of turbid water, night transport, or short transport distance (Gray et al., 2017). Partially bleached grains can hold on to residual OSL signal, in turn appearing older than the true age if multi-grain method is used (Duller, 2008). Therefore, single-grain dating helps to overcome issues related to incomplete bleaching, as the population of well-bleached grains with lowest D_e provides a means for reliably obtaining depositional ages of fluvial deposits.

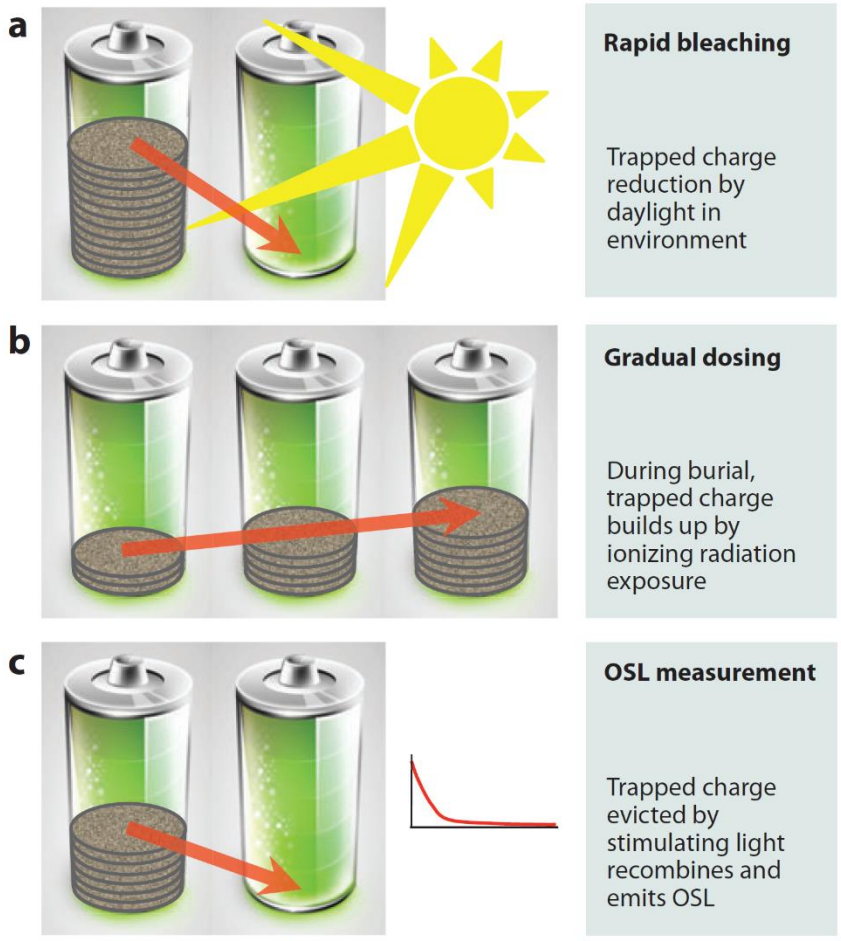

Figure 2.2 Overview of how OSL works (*From Rhodes, 2011*)**;** (A) Here, the batteries represent a grain of sand. Grains are bleached by the sun during transport, and their charge is reduced; (B) When grains are buried and shielded from light, their luminescence signal accumulates because they start to receive radiation and absorb part of the energy; (C) Under stimulation by light in the lab, the trapped energy releases photons of light –the luminescence signal. The intensity of the luminescence signal is proportional to the burial time of the sample and forms an OSL decay curve (shown to the right of the batteries).

Chapter 3 - Study Area

3.1 Introduction

Konza Prairie Biological Station (hereafter, Konza), approximately 35 km^2 in size, is a tallgrass prairie ecosystem located in the Flint Hills region of northeast Kansas. Konza is operated as a National Science Foundation-funded Long-Term Ecological Research station, with 60 watershed-level experiments to investigate the role of fire, climate, and grazing on the landscape (Knapp & Seastedt, 1998). Konza has a temperate mid-continental climate, with a mean annual air temperature of 13 degrees Celsius and annual precipitation of 835 mm. Approximately ~75% of precipitation occurs during April – September, and an average of 521 mm of snow falls each year, equaling 52 mm of liquid water (Hayden, 1998; Vero et al., 2017).

The elevation of Konza ranges from 317 – 455 m above sea level in an incised landscape, with native tallgrass throughout and gallery forests along the stream channels. The underlying bedrock consists of 14 alternating layers of fractured and jointed limestone and tightly bedded shale of Permian age (Oviatt, 1998) (Figure 3.1). The limestone layers are 1 – 2 m thick and the shale layers are 2 – 4 m thick (Macpherson, 1996). The topography features flat benches that are associated with the resistant limestone layers, and the less resistant shale layers correspond with gentle slopes (Costigan et al., 2015; Oviatt, 1998). The landscape is largely a product of weathering and fluvial erosion of streams that are tributaries the Kansas River over significant geologic time, and streams dissecting the landscape reveal the limestone and shale layers (Macpherson, 1996; Oviatt, 1998).

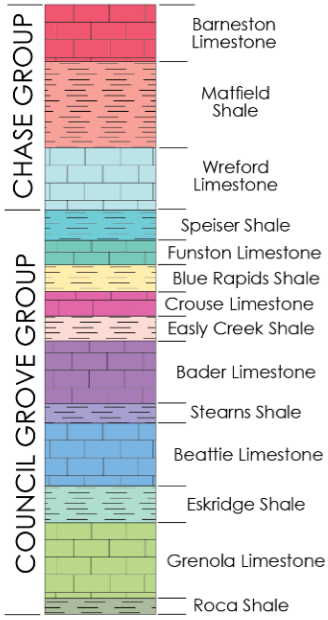

Figure 3.1 Stratigraphic column of Konza lithology (*after Oviatt, 1998*). Not drawn to scale.

Kings Creek is the main stream draining Konza (Figure 3.2A) and the only watershed located completely within Konza (Figure 3.2C). It is an intermittent stream, with perennial portions on the main trunk, and has a drainage area of ~17 km^2. Kings Creek is a mixed-alluvial bedrock river in most locations of the main trunk, with primarily bedrock channels most upstream tributary locations in the headwaters. It typically exhibits high variability in streamflow, with greatest amount of discharge typically occurring in

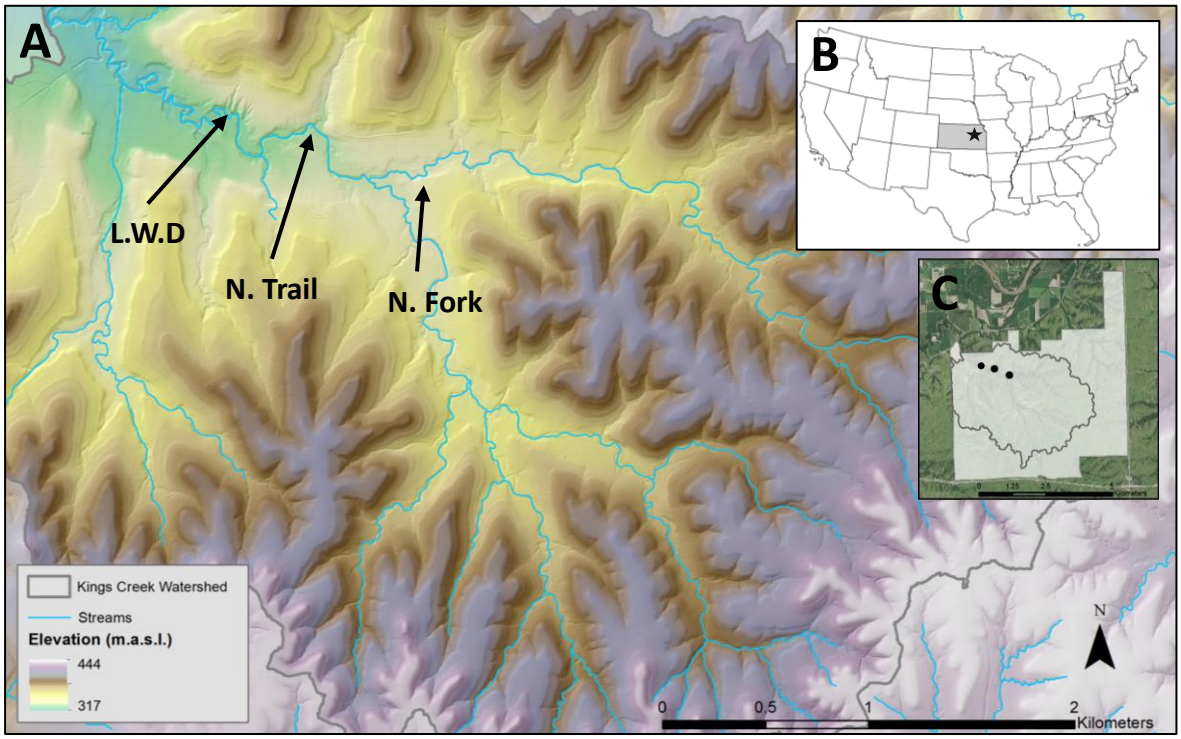

Figure 3.2 (A) DEM and overview of the Kings Creek watershed, with each study site indicated with a black arrow; (B) Location of Konza – the black star – within Kansas and the United States; (C) Extent of Konza boundary with the Kings Creek watershed within. The study sites are indicated with black dots. *DEM and aerial imagery courtesy of Konza Spatial Data Portal.*

April, May, and July and lowest average flows in the late summer and winter resulting in a near-completely dry channel (Gray et al., 1998).

I selected three reaches in Kings Creek to serve as study areas for this project (Figure 3.2A). All sites are at meander bends where the stream is actively eroding bedrock along the banks and bed. At the North Fork and Nature trail sites, modern erosion rates were measured and monitored using structure from motion photogrammetry and erosion pins installed in bedrock bed and banks. Several prominent terrace levels exist at Kings Creek (Figure 3.3A), indicating that the stream formerly occupied higher elevations and was laterally mobile. At the Large Woody Debris site, samples for OSL dating were collected from exposed terrace material from the cutbank.

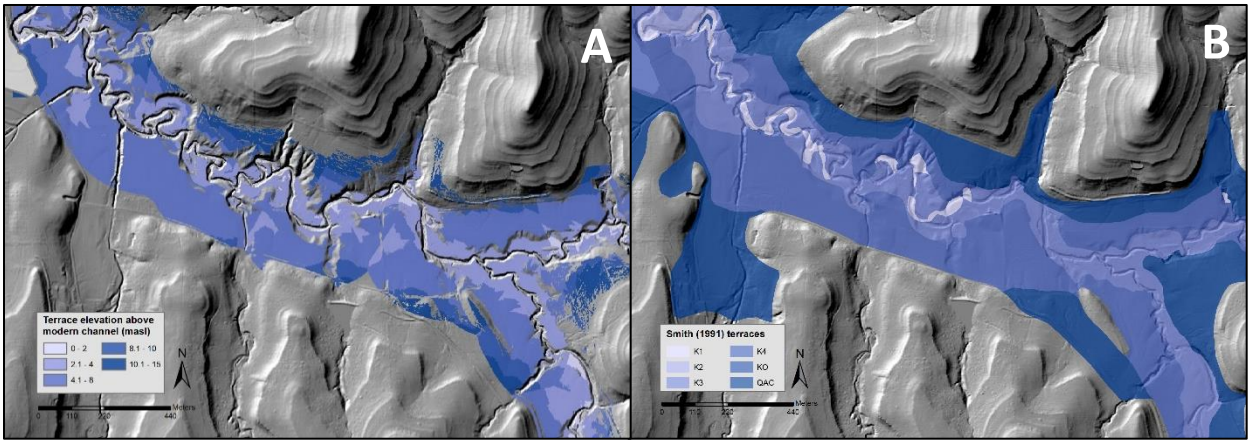

Figure 3.3 (A) Extent of terraces along the main trunk of Kings Creek ranging from 0 to 15 m above the current channel mapped using a GIS-based terrace mapping script created by A. Marcotte. Dark blue color represents the highest terrace elevation (15 m); (B) Fluvial terraces at Kings Creek as mapped by *Smith (1991)*. QAC (quaternary alluvium and colluvium deposits) are darkest blue and stratigraphically the highest terrace elevation. K1, lightest blue, is the closest in elevation to the modern channel.

3.2 North Fork Site

The first site, North Fork, is the most upstream study site (Figure 3.2) and located along the North Fork of Kings Creek. The contributing drainage area is 4.89 km^2. There are two cross-channel transects approximately 25 m apart from each other that serve as study sites to monitor modern erosion. At the upstream study area, the bank height is ~4.5 m and at the downstream study area the bank height is 3 meters. At both sites, a thin layer of colluvium (~40 – 50 cm) rests on top of limestone ~0.3 m thick, and thinner layers of shale that are ~0.10 m thick sandwiched in-between (Figure 3.4A). In-stream boulders ~0.5 to 1 m in diameter that have

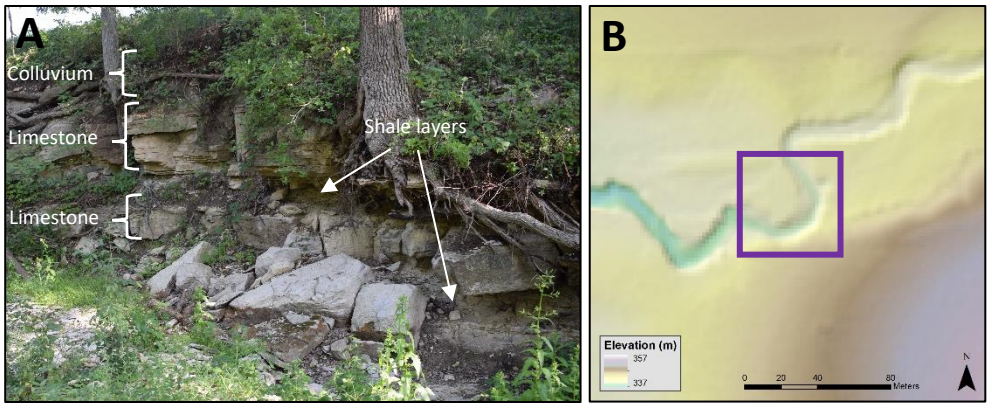

Figure 3.4 (A) Downstream study transect at the North Fork site. The white arrows and brackets indicate the layers of shale, limestone, and colluvium; (B) DEM view of the meander bend of the North Fork site (purple square).

collapsed from the North Fork is limestone with some alluvial cover that tends to be gravel- and small cobble-sized.

3.3 Nature Trail Site

The Nature Trail site is located approximately 770 meters downstream of the North Fork site and located on the main trunk of Kings Creek (Figure 3.2A). The contributing upstream drainage area is 11.22 km^2. Here, there are also two cross-channel transects approximately 25 meters apart from each other that serve as study locations at this reach. The bank height for the entire reach is ~6.5 meters. At both the upstream and downstream cross sections, there is a thick layer of colluvium (~ 3 m) resting atop of the alternating shale and limestone layers that are both ~30 cm in thickness (Figure 3.5A). The channel bed is limestone, with intermittent alluvial cover.

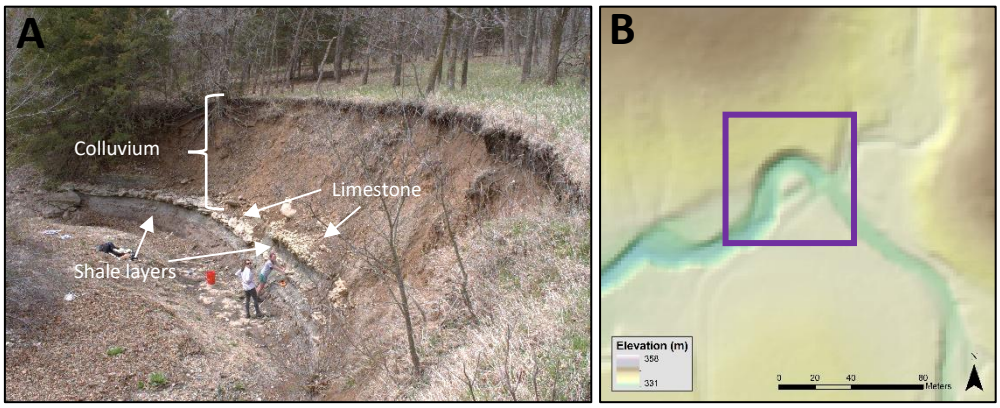

Figure 3.5 (A) Overview of the entire study reach at the Nature Trail site. The white arrows and brackets indicate the layers of shale, limestone, and colluvium; (B) DEM view of the meander bend of the Nature Trail site (purple square).

3.4 Large Woody Debris Site

The Large Woody Debris (LWD) site is located approximately ~660 m downstream of the Nature Trail site on the main trunk of Kings Creek (Figure 3.2A). The contributing drainage area is 12.3 km^2. A thick layer (~2 m) of alluvium caps exposed bedrock in the bank. The alluvial material has alternating layers of imbricated cobbles and fine-grained floodplain deposits, indicating that this site was formerly occupied by the stream and is a strath terrace. Four samples for optically stimulated luminescence were collected from the alluvium exposed on

the channel bank: three samples at an upstream location and one sample ~20 m downstream (Figure 3.6A).

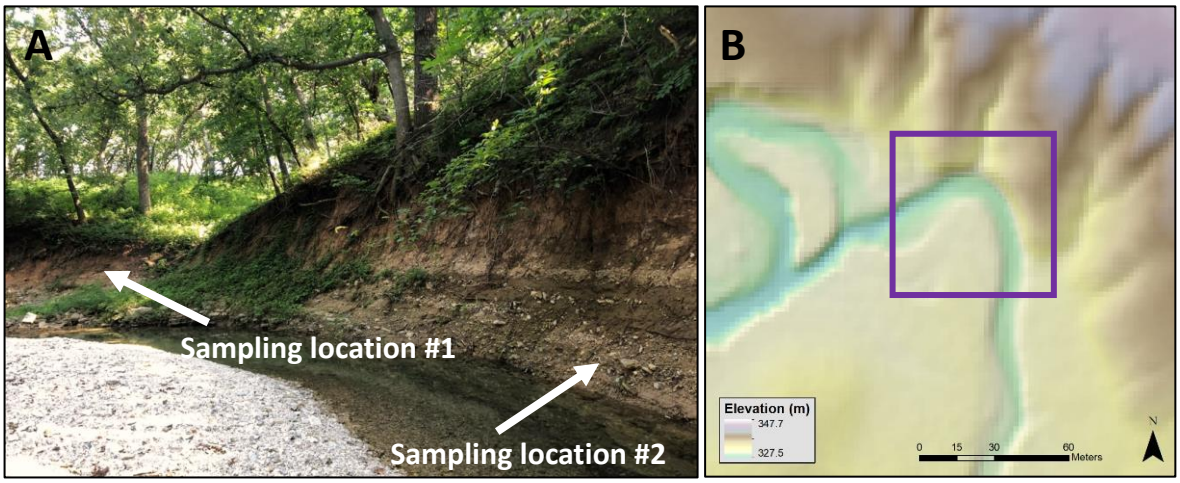

Figure 3.6 (A) OSL sampling locations #1 and #2, indicated with white arrows, along the meander bend at the Large Woody Debris site; (B) DEM view of the meander bend of the Large Woody Debris Site (purple square).

At the downstream sampling location – sampling location #1 – the channel bank is ~4 m high. The sample, KNZ001, was taken 1.7 m above the bedrock. The fluvial deposits consist of mostly medium- to large-sized cobbles, and a few small boulders. The sampled material itself is fine-grained floodplain material and some small gravel-sized grains.

At the upstream sampling location – sampling location #2 – the channel bank is ~4.5 m high. There is a ~2.5 m layer of colluvium that rests on top of a 2 m layer of alluvium with alternating imbricated fluvially deposited material and fine-grained floodplain material. Samples KNZ003, KNZ004, and KNZ005 were taken from the fine-grained material due to the difficulties and risk of bleaching grains involved in collecting OSL samples from gravel.

KNZ003 is the stratigraphically lowest sample, obtained ~0.20 m above the bedrock. The sample collection layer is ~18 cm thick, consisting of mostly clay sized materials and lenses of sand. It is sandwiched between two layers of gravel and small cobble-sized layers. KNZ004 is separated from KNZ003 by a 0.6 m-thick layer of coarse sand and cobble-sized material. The KNZ004 sample layer is 1.05 m above the bedrock. A ~0.12 m-thick cobbley layer separates the KNZ005 sampling layer from KNZ004. The KNZ005 sample layer is 1.55 m above the bedrock. The sample was taken from silty clay layer that is ~0.15 m-thick, although there were some small gravel and fine sand materials throughout the layer as well.

Chapter 4 - Methods: Erosion Pins and Structure from Motion

4.1 Erosion Pin Measurements

Erosion pins installed in the channel banks and beds at the Nature Trail and North Fork sites were used to address research question #1. At both cross sections at both study sites, 25 erosion pins were installed horizontally in the bedrock channel banks and 11 were installed vertically in the bedrock beds. Erosion pins at the Nature Trail site were installed on April 26, 2018 and erosion pins at the North Fork site were installed on May 16, 2018. Tables 6.1, 6.2, and 6.3 give an overview of pin locations relative to the channel bed. At each transect, one or more erosion pins were placed in each of the limestone and shale layers rather than at equal spacing intervals in order to capture variability in erosion rate within lithology sequences (Figure 4.1). Pins were also placed into the in-stream limestone boulders at the North Fork site. I used 80 mm-long nails to serve as erosion pins for limestone layers and 160 mm-long nails in the shale layers because shorter pins are at higher risk to being lost through erosion (Couper & Maddock, 2001). Both limestone and shale pins are ~6.5 mm in diameter.

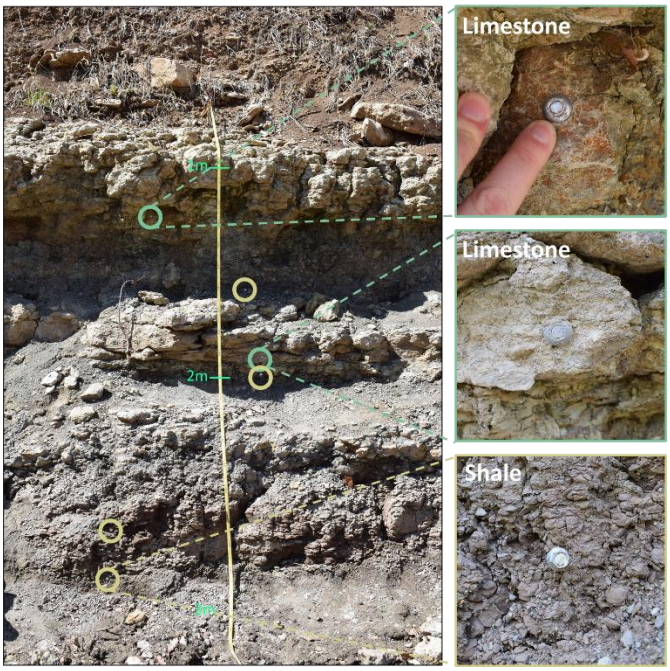

Figure 4.1 Example of an erosion pin transect at the upstream Nature Trail site.

Erosion pins were measured six times at the North Fork site and five times at the upstream Nature Trail site over the 21-month study period. I originally planned to measure each erosion pin every six weeks; however, due to an uncharacteristically wet year, flow conditions at

Kings Creek were oftentimes unsafe for me to wade through the creek to collect data. I instead measured erosion pins after flow events whenever possible to capture the effects. Bed pins could sometimes not be located due to sediment or moss cover, and thus were infrequently measured. Erosion pins were measured using Vernier calipers (accurate within 0.05 mm). The measured length of the exposed pin relative to the channel bank is the total erosion (or possible deposition in the case of negative readings) between each visit. I measured each pin from the same location around the pin each survey to reduce introduction of measurement errors. Simon et al., (1999) estimates that pin readings for rebar-sized erosion pins (~9 mm diameter) are accurate to within ± 5 mm based on measurements conducted by different users during one day. Harden et al., (2010) found measurement error for steel rods serving as erosion pins (25-cm long, 3.2 mm in diameter) to have a range of ~3 cm. However, I conducted my own accuracy experiment by measuring a pin five separate times and found that the accuracy is approximately ± 0.44 mm. Additionally, I was the only person who measured the pins for this study, therefore operator variant measurement errors observed in Simon et al. (1999) should not apply to this study.

Moultrie Trail Cameras were installed facing the stream bank at the Nature Trail and North Fork sites. The trail cameras took photos at 30-minute intervals for the duration of the study period. The trail camera photos were paired with discharge data to determine the water stage during high flow events. The photos also aided in assessment of contributing bank erosion mechanisms (see Appendix A).

4.2 Structure from Motion Photogrammetry

Structure-from-motion photogrammetry (hereafter, SfM) was used to identify patterns of erosion and deposition along the channel banks at the North Fork and Nature Trail site to address research question #1. Each survey was executed in a systematic way such that I began by capturing the entire channel bank from several different locations, then gradually moved closer to the bank while also shifting the camera angle to capture different bank features to ensure adequate image overlap (Micheletti et al., 2015; Dietrich, 2016). I also maintained a fixed focal length lens for each survey, either 24 or 35 mm depending on sunshine angle, to help minimize distortion (Mosbrucker et al., 2017). All photos were acquired using a Nikon D5300 Digital Single Lens

Figure 4.2 A ‘marker’ generated by Agisoft Photoscan.

Reflex (DSLR) camera. Photos were captured in .NEF format (Nikon's raw format), then converted to .DNG format using Adobe DNG Converter to process photos in Agisoft Photoscan.

I used 'markers' (Figure 4.2) generated in Agisoft Photoscan (SfM photo alignment software) and glued them to poster board to serve as an arbitrary coordinate system. Each marker was placed througout the study sites so as not to cover up important features, but also in locations that were spread out far enough from each other across the bank. Each marker is a black and white target, each with a different pattern, which helps Agisoft Photoscan easily identify the maker and aids with the photo alignment process since there are common overlapping features in each photo. The distance between the center dot of each marker helps with giving a scale to the dense point clouds that are generated in Agisoft Photoscan.

4.2.1 SfM Image Processing

All photosets were processed in Agisoft PhotoScan Professional v1.4.4 (Agisoft, 2018). Agisoft PhotoScan is an SfM software that uses automated image matching algorithms to produce an image-based 3D model. The processing workflow consists of seven major steps:

1) Estimate image quality: Images with a quality value of less than 0.5 units are removed from the photoset. I also looked through the photosets to eliminate additional poor-quality images.
2) Align photos: this stage is when PhotoScan finds the camera position and orientation of each photo in order to construct a sparse point cloud model. Alignment parameters were chosen as follows:
    a. Accuracy: High – high accuracy helped produce a more accurate sparse point cloud in the initial stages of processes than a medium quality (Morgan et al., 2017).
    b. Pair preselection: Generic
    c. Key point limit: 40,000 – This represents the upper limit of feature points found in every imaged to be considered during processing. Using zero will result in a large number of points and likely less reliable points since there is no limit to the number of key points PhotoScan can identify.
    d. Tie point limit: 4,000 – This represents the upper limit of matching points in every image.
    e. Adaptive camera model fitting: Disabled

3) Assign markers and quality check alignment results: PhotoScan automatically detects most markers, which helps when adjusting the sparse point cloud if photos are incorrectly positioned.
4) Assign scale to point cloud using the markers
5) Build dense point cloud:
    a. Quality: Medium – Medium was chosen as an ideal choice between quality and processing time because high and ultra-high-quality settings require significant computer memory and processing time upwards of seven days.
6) Export dense point cloud as .LAS format for analysis in CloudCompare.

4.3 Cloud Compare

I used CloudCompare v2.10.2 (CloudCompare, 2019) to align point clouds from successive surveys, April/May 2018 to May 2019 and May 2019 to October 2019, respectively, from the Nature Trail site and the downstream site at North Fork. I manually aligned the point clouds by assigning three or more common points in each point cloud, such as visible erosion pins or points on large limestone boulders, to serve as alignment points. Once the point clouds were aligned, I used the Model to Model Multi-Scale Cloud Compare plug-in (hereafter, M3C2) in CloudCompare to compare distances between two point clouds (Lague et al., 2013). The M3C2 algorithm is better suited for vertical surfaces than DEMs, such as channel banks, because DEMs cannot describe steepness and do not cope with overhanging parts (Lague et al., 2013).

The M3C2 algorithm calculates the difference between two point clouds along a cylinder at a given normal scale. The normal scale is the radius of a sphere in which neighboring points will be used to calculate a best plane fit. The radius of the cylinder is called the projection scale and the height of the cylinder is called maximum depth. I used the whole cloud for all comparisons, and normal scales of 0.1 m in diameter, projection scales of 0.025 m, and a maximum depth of 1 m.

Chapter 5 - Luminescence Dating: Methods and Results

5.1 Introduction

I used single grain optically stimulated luminescence (hereafter, OSL) dating of quartz grains at the Large Woody Debris site to determine the depositional age of fluvial deposits sourced from a strath terrace, which addresses research question #2.

5.2 Sample Collection

The first samples, KNZ001 and KNZ002, were obtained on June 17, 2019 at sampling location #1 from a single stratigraphic layer to determine if fluvial sediment from Kings Creek would yield enough high-quality quartz to perform single grain OSL dating. KNZ001 and KNZ002 were eventually combined as one sample, KNZ001, prior to the HF step (see section 5.3 for explanation) due to a limited amount of quartz grains in both samples for OSL measurements. Three additional samples, KNZ003, -004, and -005, were taken upstream of KNZ001 at sampling location #2 on August 28, 2019 in a vertical profile after determining from KNZ001 that the quartz grains at Konza were suitable for OSL dating

All samples were collected in the field with a black PVC tube (~30 cm long, ~6 cm diameter) to prevent sunlight from bleaching the sediment grains. Loose sediment was cleared from the face of the channel bank, revealing a fresh face of sediment. A tube was hammered into the bank horizontally and then ends were sealed with foam discs upon extraction. It is important that the material in the tube does not get mixed because the material on the interior part of the tube has been exposed to sunlight since it was last transported, and therefore is not bleached. Once both ends of the tube were capped with foam, I wrapped several layers of black electric tape to seal the ends and put the tube in two black plastic bags as a final measure to shield the sample from any potential light source.

5.3 Sample Preparation

Samples were processed at the Desert Research Institute Luminescence Laboratory in Reno, Nevada, U.S.A. under dim red illumination so as not to light contaminate samples. KNZ001 was processed June to July 2019, and KNZ003, -004, and -005 were processed October to November 2019.

Sediment at both ends of the tube (~3 cm) were carefully removed due to possible light contamination during sampling. This portion of the sample was used to determine the

geochemistry of the sample for environmental dose rate (explained in section 5.5). The sample was dried at 50°C to determine the water content of the sample at the time of sample collection. Water content is also used in environmental dose rate determination.

The remainder of each sample was prepared in the laboratory for OSL measurements. Because the samples had high clay and silt sized particles, samples were given a sodium pyrophosphate decahydrate ($Na_4P_2O_7 \cdot 10H_2O$) for one day to reduce clumping of fine material. Samples were then wet sieved to target grains 90 to 125 µm in diameter. The grains were given 10% hydrochloric acid (HCl) to remove carbonates for 24 hours, and then 30% hydrogen peroxide (H_2O_2) for 24 hours to remove any remaining organic material. A hand-magnet was used to separate heavy minerals out of the quartz. The non-magnetic fractions of each sample went through a two-step density liquid separation using lithium heteropolytunstates (LST) to separate the quartz grains ($2.62 < \rho < 2.68$ g/cm^3) from feldspar grains. The quartz grains were etched in 48% hydrofluoric acid (HF) for 60 minutes to remove the outer alpha-irradiated rim of the quartz grains and to remove any contaminating feldspars that remain after density separation. Following the HF treatment, samples were treated with HCl 10% for three hours to remove any precipitated fluorides and re-sieved at the target fraction (90-125 µm).

5.4 Measurement of Equivalent Dose

All measurements of quartz grains were made on two DA-20 Risø TL/OSL readers equipped with green and IR laser single-grain dating attachments and 90Sr/90Y beta source with dose rates ~0.13 gray(Gy)/s and ~0.11 Gy/s. For single grain OSL measurements, quartz grains were loaded onto aluminum discs with 100 holes, each 300 µm wide. Due to the small size of quartz grains in my samples (90-125 µm), each hole had ~3-10 grains in it. This is commonly referred to as 'pseudo' single grain or 'very small' aliquot dating (Arnold et al., 2012), where each hole containing grains is an aliquot.

All equivalent dose (D_e) values were obtained following the single aliquot regenerative-dose (SAR) protocol (Murray & Wintle, 2000; Wintle & Murray, 2006). The SAR procedure involves repeated measurements of an aliquot to first determine the natural OSL signal, which is the signal accumulated during the time sediment was buried, and then to determine the aliquot's response to given doses of radiation (called a regenerative dose). The SAR protocol is outlined in Table 5.1. Steps 1 – 7 may be repeated as many times as desired, administering a higher regenerative dose each round. The preheat removes unstable charge from electron traps before

OSL measurements. Because my samples were bright (i.e., giving off a lot of luminescence signal), the SAR sequence I used consisted of regenerative doses ranging from 50 seconds to 5000 seconds to generate the SAR growth curve (Figure 5.1B).

Table 5.1 SAR protocol applied in this study.

Step	Treatment
1	Natural/Regenerative Dose
2	Preheat (220°C , 10 seconds)
3	Measure natural or regenerative dose (125°C, 1 second)
4	Administer test dose
5	Cutheat (160°C, 10 seconds)
6	Measure test dose (125°C, 1 second)
7	Record OSL decay curve (220°C, 100 seconds)
8	Return to Step 1

5.5 Environmental Dose Rate

The dose rate (D_r) is an essential part of the OSL age determination (Durcan et al., 2015; Rhodes, 2011), which is a measurement of how quickly luminescence signal is accumulates in sediments after exposure to sunlight (Walker, 2005). This is the measurement of radiation received by a sample over its entire burial history from alpha and beta particles, gamma rays, and cosmic rays. The alpha, beta, and gamma dose rates originate from naturally occurring radioactive elements thorium (Th), uranium (U), and potassium (K) that make up and surround the sample. The geographic location, altitude, and burial depth will influence the intensity of cosmic rays received by the sample (Walker, 2005).

The dried portion of each sample taken from the end of the tubes was pulverized into fine powder. Approximately one gram from each sample was sent to ALS Vancouver in British Columbia, Canada for ICP-MS/-AES to determine the geochemistry and concentration radioactive elements of each sample. The environmental dose rates were calculated using DRAC v1.2 (Dose Rate and Age Calculator; Durcan et al., 2015), which uses the above components as well as the grain size, water content, altitude, burial depth, and geographic location of the sample to calculate the total D_r. The environmental dose rate for each sample is given in 5.2. Once the dose rate is established, the OSL age can be obtained by dividing the equivalent dose from the does rate.

Table 5.2 Radioactive nuclide concentrations and the environmental dose rate for each of the samples.

Sample number	U[a] (ppm)	Th[a] (ppm)	K[a] (%)	Cosmic dose rate[b] (Gy/ka)	Total dose rate[c] (Gy/ka)
KNZ001	3.58	12.425	2.44	0.161	4.083 ± 0.231
KNZ003	2.89	8.45	1.74	0.14	2.986 ± 0.166
KNZ004	3.56	11.3	2.11	0.154	3.687 ± 0.204
KNZ005	3.38	10.3	1.75	0.163	3.25 ± 0.175

[a] Elemental concentrations from ICP-MS/-AES
[b] Cosmic dose rates (Gy/ka) are calculated according to Prescott & Hutton, 1994
[c] Dose rates (Gy/ka) were calculated using the conversion factors of Liritzis et al., 2013

Water content of the sample over its entire burial history needs to be considered for dose rate determination, as water absorbs alpha, beta, and gamma rays thus affecting the environmental dose rate of a sample and the calculated age of the sample (Li et al., 2013). Water content, expressed as a percentage, was determined by subtracting the mass of the wet sample from the mass of the sample after drying. Apart from KNZ001 (water content 7%), the samples collected in August had a higher water content (water content > ~20%), likely due to the high amount of precipitation in the few days prior to sample collection (Figure 6.1).

Laboratory measured water contents may not be representative of the burial water content of a sample, as water content can change drastically over time from initial deposition. Water contents may also be over- or underestimated if, for example, there has been recent precipitation event or a long span of time with no precipitation (Nelson et al., 2019). Because of the modern arid climate and the uncertainty in each sample's environmental history, a lower water content of 7% was assumed for KNZ003, KNZ004, and KNZ005 with an assigned error of 50%. Assuming a lower water content will ultimately result in minimizing the age of the sample, rather than overestimating the age of the sample.

5.6 Rejection Criteria

After measurement of the samples on the Risø readers, all aliquots were screened in Analyst version 4.31.9 (Duller, 2016). Aliquots were accepted based on the following acceptance criteria: (1) recuperated OSL signal less than 5% of natural signal; (2) recycling ratio between 0.8 and 1.2 (20% of unity); (3) OSL infrared (IR) stimulation ratio between 0.8 and 1.2 (response to IR stimulation could indicate feldspar contamination). The dose response curve of each aliquot

was fit using exponential + linear curve and a measurement error of 1.5%. Aliquots were rejected if they had a poor dose response curve that did not pass through origin or if the curve did not fit well to the data points. Aliquots were also rejected if the intersection of the Lx/Tx – the ratio of luminescence signal to the test dose – was drawn beyond the furthest regenerative dose point indicating that the sample was saturated with luminescence signal. The De is plotted where the natural signal falls on the curve (Figure 5.1).

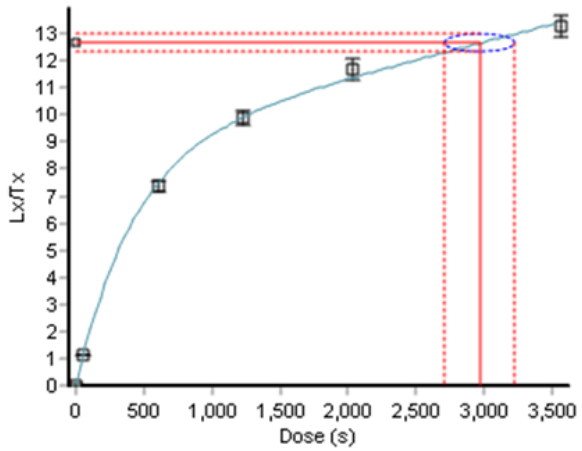

Figure 5.1 Growth curve from a KNZ003 aliquot that meets passing criteria.

5.7 Statistical Age Modeling

Single grain results were analyzed using the Luminescence package (Kreutzer et al., 2012) in R statistical software. The D_e estimate for each sample was calculated using the 3-parameter minimum age model (MAM) (Galbraith & Roberts, 2012). MAM assumes that the D_e distribution of each sample are from a truncated normal distribution. The truncated peak is the population with the lowest D_e values, and therefore the best-bleached portion, which is used to calculate the D_e estimate. MAM is often the most suitable statistical age model for samples that may not have been fully bleached prior to deposition (Galbraith & Roberts, 2012), such as fluvial samples that may have been partially bleached during transport. Figure 5.2 shows D_e distribution of each sample. The dots are D_e values of accepted aliquots plotted in rank order with standard error bars, and the solid line is the kernel density estimate (KDE) of the D_e values.

5.8 OSL Ages

The OSL age of the sample is determined by dividing the equivalent dose (D_e) by the dose rate (D_r). The OSL ages of the fluvial deposits are shown in Figure 5.3 and Table 5.3. OSL samples KNZ003, KNZ004, and KNZ005, collected at sampling location #2, yield ages of 30.8 ± 4.8 ka, 36.64 ± 4.36 ka, and 19.910 ± 3.67 ka, respectively. The samples KNZ003 and KNZ004 do not fall in the expected chronological order, but since the two sample ages overlap given the error, the ages are approximately the same. However, the age of the KNZ003 deposit must be older than KNZ004 given the law of superposition. OSL sample KNZ001, collected at sampling location #1, has an age of 19.84 ± 2.79 ka.

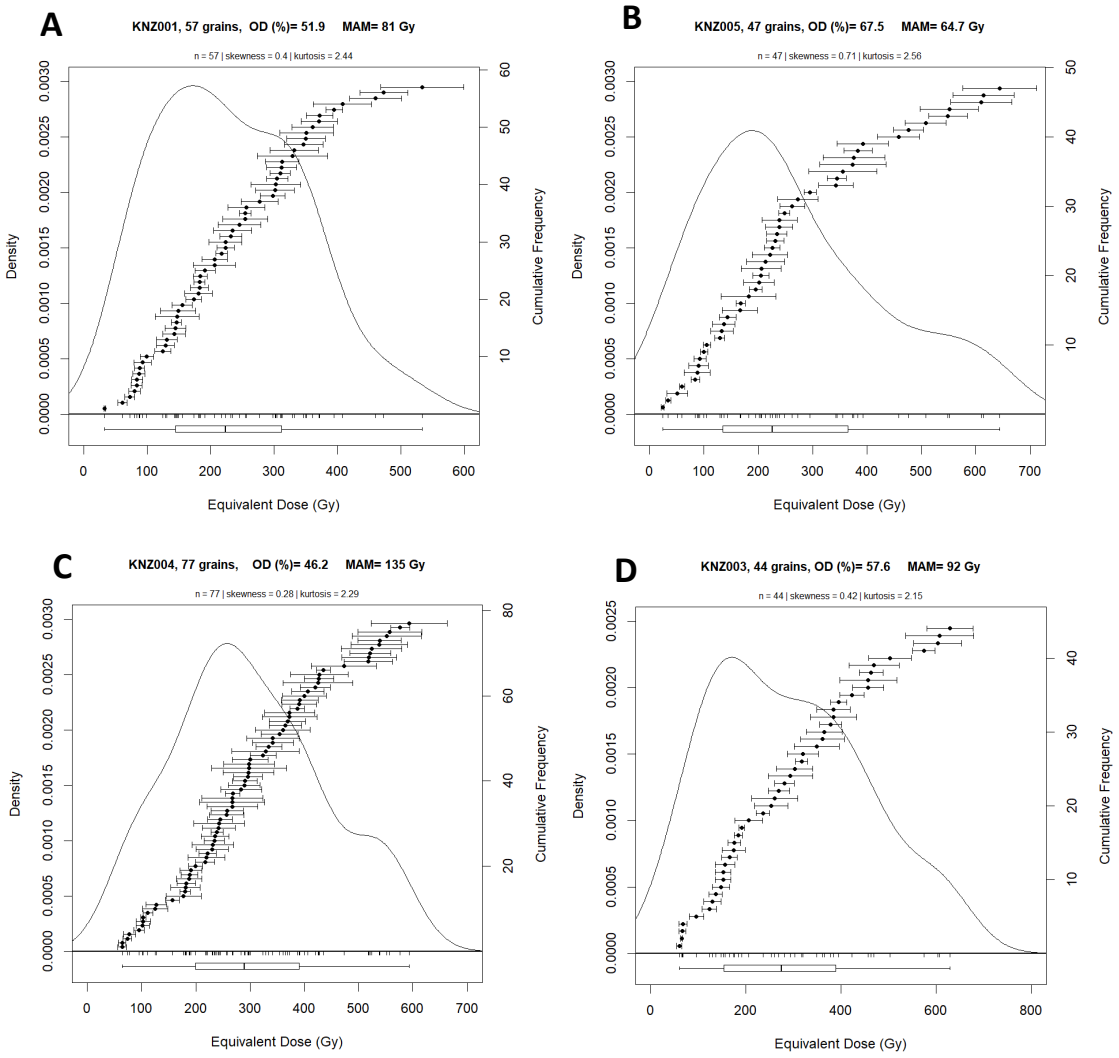

Figure 5. 2 Kernel density estimate (KDE) plots for each sample. The dots represent the equivalent dose in rank order with standard error bars. The solid black line is the KDE estimate of the De values. (A) KDE plot for sample KNZ001; (B) KDE plot for sample KNZ005; (C) KDE plot for sample KNZ004; (D) KDE plot for sample KNZ003.

Figure 5.3 Left: OSL age of KNZ001 from sampling location #1; Right: OSL ages of KNZ003, KNZ004, and KNZ005 from the depositional layers at sampling location #2.

Table 5.3 Summary of location data, dose rate, equivalent dose, and OSL age estimates for each sample

Sample Location	Sample ID	Depth (m)	Location (decimal degrees)	Altitude (m)	N accepted (N analyzed)	Over-dispersion (%)	MAM De (Gy)	Total dose rate (Gy/ka)	Age (ka)
1	KNZ001	2.57	39.104497, -96.60001	327.25	57 (900)	51.9	81 ± 10.68	4.083 ± 0.231	19.84 ± 2.847
2	KNZ003	3.75	39.104405 -96.59979	325	44 (1200)	57.6	91.96 ± 13.67	2.986 ± 0.166	30.797 ± 4.889
	KNZ004	2.95		325.5	77 (1300)	46.2	135.09 ± 14.71	3.687 ± 0.204	36.64 ± 4.477
	KNZ005	2.45		326.5	47 (800)	67.5	64.69 ± 11.55	3.25 ± 0.175	19.907 ± 3.713

Chapter 6 - Erosion Pins and Structure from Motion Results

6.1 Erosion Pins

The erosion pin measurements (Tables 6.1, 6.2, and 6.3) shows the measurements for every survey at each pin. Some bank and bed pins were not measured because I could not find them, either due to debris cover or the pin was missing. In other instances, I could visually spot the pin but could not reasonably reach the pin to measure it. Erosion pins were not measured at the downstream transect at the North Fork site because a limestone block collapsed in-stream and covered all the bank pins. At both sites, seven of the 12 shale pins in the channel bank eventually were completely eroded and removed from the channel banks, and three of the 11 limestone pins in the channel banks and in-stream boulders were completely eroded and removed. If a pin was missing, then the whole length of the pin was assumed eroded. Figures 6.3, 6.4, and 6.5 show the cumulative erosion measured at each erosion pin in the channel banks at each site.

Table 6.1 Erosion pin measurements (mm) and the corresponding date from the upstream Nature Trail site. Elevation is the distance of the pin from the channel bed. S lithology indicates the pin is in shale and LS indicates the pin is in limestone.

Pin #	Elevation (m)	Lith.	11/21/18	08/09/18	10/27/19	11/16/19	01/26/20
1	2.07	LS	0	0	0	0	0
2	1.76	S	♦	24.1	60.05	62.1	59.25
3	1.42	S/LS	0	☒	☒	☒	☒
4	1.32	S	16.75	44.9	45.95	47.7	49.3
5	0.95	S	14.6	108.65	♦	110.1	113.6
6	0.65	S	48.8	●	☒	☒	☒
7	0.48	S	♦	☒	☒	☒	☒

● - Pin spotted visually, but couldn't measure because water was too deep and/or cold; ♦ - Pin not found visually not measured because I couldn't find it due to sediment cover, turbid water or moss cover, etc; ☒ = Pin missing

Table 6.2 Erosion pin measurements (mm) and the corresponding date from the downstream Nature Trail site. Elevation is the distance of the pin from the channel bed. S lithology indicates the pin is in shale and LS indicates the pin is in limestone. Pins 1, 2, and 3 are all at the same elevation, but at different facing locations upstream and downstream.

Pin #	Elevation (m)	Lith.	11/21/18	05/22/19	08/09/18	10/27/19	11/16/19	01/26/20
1	1.53	LS	0	0	0	0	0	0
2	1.53	LS	0	0	0	0	0	0
3	1.53	LS	0	0	0	0	0	0
4	1.19	S	17.65	⊠	⊠	⊠	⊠	⊠
5	0.81	S	38.95	⊠	⊠	⊠	⊠	⊠
6	0.7	S	49.35	94.25	80.6	73.3	86.9	85.6
7	0.47	S	19.3	●	114.1	●	131.85	70.7
8	0.43	S	32.45	93.9	100.1	91.4	101.45	87.9

Table 6.3 Erosion pin measurements (mm) and the corresponding date from upstream North Fork site. Elevation is the distance of the pin from the channel bed. S lithology indicates the pin is in shale, LS indicates the pin is in limestone, and LSB indications the pin is in an in-stream limestone boulder

Pin	Elevation (m)	Lith.	11/21/18	05/19/19	08/09/18	10/6/19	11/16/19	01/26/20
1	0.66	LS	0	0	0	0	0	0
2	0.54	LS	0	0	0	0	0	0
3	0.5	LS	1.70	⊠	⊠	⊠	⊠	⊠
4	0.4	LSB	0	0	45.5	◉	46.6	44.8
5	0.29	S	6.4	106.3	104.9	108.15	100.05	⊠
6	0.18	S	0	♦	90.55	120.05	99.5	⊠
7	0.05	S	25.0	⊠	⊠	⊠	⊠	⊠
8	-0.24	LSB	20.85	◉	30.05	44.45	44.6	46.5
9	-0.16	LSB	0	29.4	⊠	⊠	⊠	⊠
10	-0.08	LSB	0	33.1	⊠	⊠	⊠	⊠
Bed pins								
1		LS	♦	♦	♦	♦	14.0	♦
2		LS	♦	◉	12.40	♦	♦	♦
3		LS	♦	♦	♦	♦	♦	♦

● - Pin spotted visually, but couldn't measure because water was too deep and/or cold; ♦ - Pin not found visually not measured because I couldn't find it due to sediment cover, turbid water or moss cover; ◉ - no visible change and therefore not measured; ⊠ - Pin missing

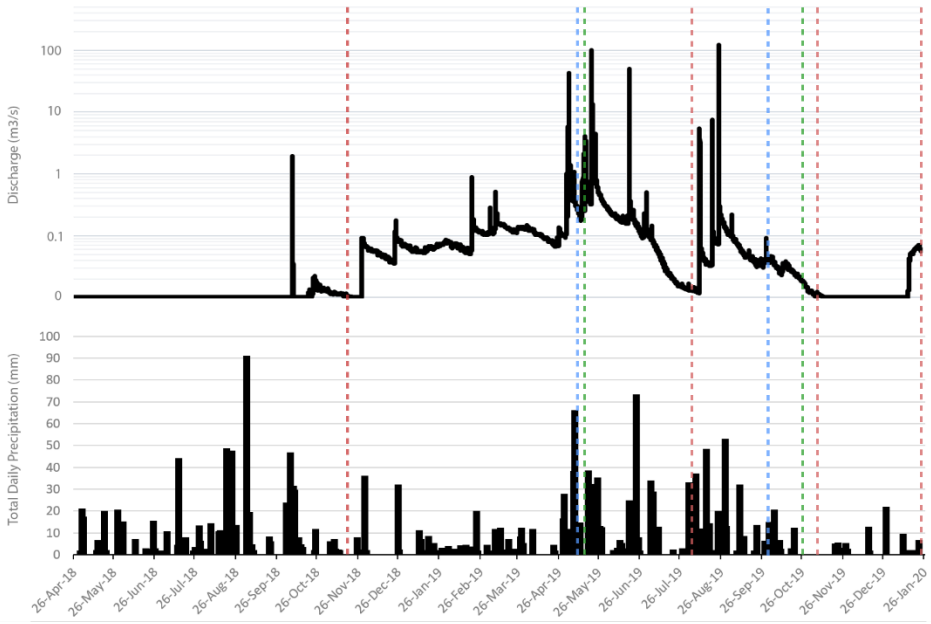

Figure 6.1 Discharge (top) and daily precipitation (bottom) for the duration of this project. Green dotted line indicates erosion pin survey at Nature Trail site, blue dotted line indicates erosion pin survey at North Fork site, and red dotted line indicates surveys at both sites in the same day. *Discharge data courtesy of USGS stream gauge #06879650. Precipitation courtesy of Konza Data Catalog (Blair, 2019).*

6.1.1 Shale Erosion

The highest erosion values occurred in the shale layers. The total shale erosion amounts over the 21-month long study range from 3.3 mm to 113 mm. The amount of erosion was incremental in between each survey compared to limestone, and plucking was likely the mechanism because of the slakey nature of shale. Erosion pin measurements show that there is substantial erosion of shale, especially near the bottom of the bank (Figures 6.3, 6.4, and 6.5). The average annual rate of shale lateral erosion at both sites ranges from 38.81 – 53.41 mm/yr. This was calculated by averaging the cumulative erosion (in mm) over the study period at each shale pin and dividing that by the number of days in the study (620 days), giving an erosion rate of mm/day. This daily erosion rate was multiplied by 365 divided by 1 mm to give a yearly erosion rate. Under the conditions of the summer months (May – October 2019) with several high flow events (Figure 6.1), the average annual rate would range from 179.29 – 276.01 mm/yr. Most measured erosion pin values were positive and correlate to bank retreat; however, a few readings were negative (a total decrease in the length of exposed pin), indicating deposition in the area around the pin.

Negative readings were recorded at both sites during the August 2019 survey, and at the Nature Trail site during October. The negative readings during the summer are not a result of freeze thaw cycles because temperatures below -5°C over several consecutive days are needed to be effective (e.g., Jugie et al., 2018). Rather, the negative readings are likely a result of bank material eroded from the upper bank and being deposited at the toe of the bank (Figure 6.8 and 6.9). The shale measurements at North Fork on November 2019 yielded negative values. At this time, the water stage had gone down, causing the shale to dry out and become less cohesive, which could lead to enhanced deposition in the friable shales. By the January 2020 survey, all remaining pins in the shale layers at the North Fork site had gone missing.

6.1.2 Limestone Erosion

The greatest limestone erosion occurred in the in-stream boulders close to the channel bed at North Fork (Figure 6.5). The observed mechanism of limestone erosion is plucking because blocks from the surface of the rock were missing. It is possible that abrasion contributed to the weakening and fracturing of the rock (Figure 6.2), which would make plucking more efficient. Erosion in limestone is not gradual, rather it is plucked away rapidly, which likely occurs during high flow events. The recorded limestone erosion over the measurement period ranges from 0 mm to 46.5 mm (see Tables 6.1, 6.2 and 6.3). Not including the 0 mm measurements in calculations, the average annual limestone lateral erosion rate is 20.82 mm/yr, and 96.80 mm/yr during the summer months (May – October 2019). These rates were calculated using the same method as the shale erosion rates. No limestone erosion occurred at the downstream Nature Trail site (Table 6.2 and Figure 6.3), likely because the erosion pins are at the top of the bank and are seldom under attack from water or sediment impacts. Similarly the

Figure 6.2 Limestone layer in the channel bank at the upstream North Fork site on May 16, 2018 (Left) and November 16, 2019 (right) with loosely held rock fragments, likely as the result of abrasion.

erosion pins installed in the limestone at the top of the banks at North Fork lacked measurable amounts of erosion (Table 6.3 and Figure 6.5).

An additional observed lateral erosion mechanism is mass wasting of limestone blocks into the stream. The first instance occurred on December 23 when a large limestone boulder ~1.5 m in diameter at the downstream North Fork site collapsed into the stream (Figure 6.6). As a result, erosion pins at this site are buried underneath this boulder. The cause of collapse is unknown, but it was likely due to the severe undercutting of the bank before the start of this study.

6.1.3 Bed Pin Measurements

There were four bed pins at each transect at the Nature Trail site, and three bed pins at each transect at the North Fork site. Erosion pins installed in the channel beds were often difficult to locate due to sediment and debris cover and were measured with less frequency compared to the bank pins. Bed pins were never measured at the Nature Trail site because of the constant high-water stage. Instances where the pins were located but not measured because there was no visible erosion are also reported in Tables 6.1 and 6.2. At the North Fork upstream site, bed pins were measured twice. Erosion of the limestone channel bed occurred at the upstream North Fork site (Table 6.3) and revealed a shale bed observed at the November 2019 survey.

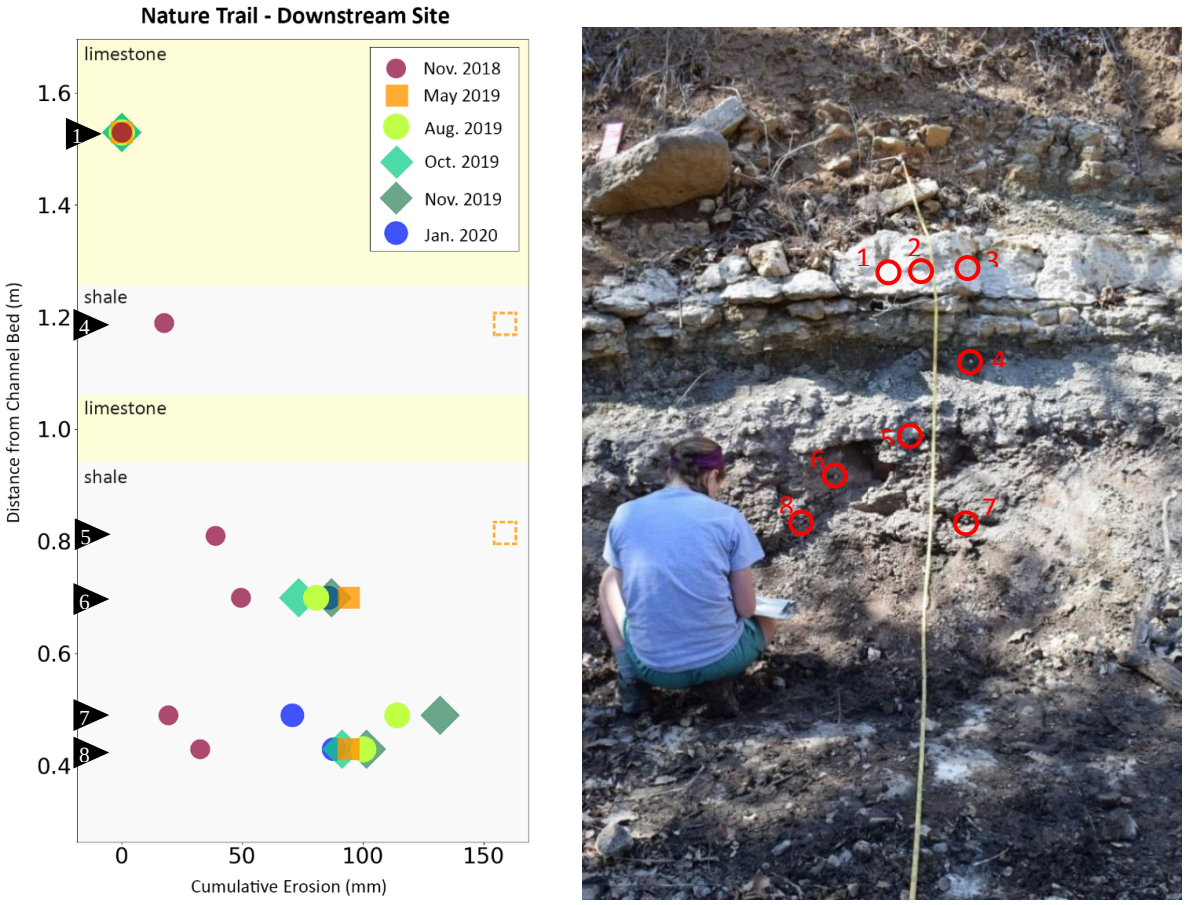

Figure 6.3 Measurement of cumulative erosion at each erosion pin at the downstream Nature Trail site since installment in April 2018. The hollow shape and color indicate the month that the pin went missing. The red circles and number correspond to the pin number in the black triangle on the y-axis of the graph.

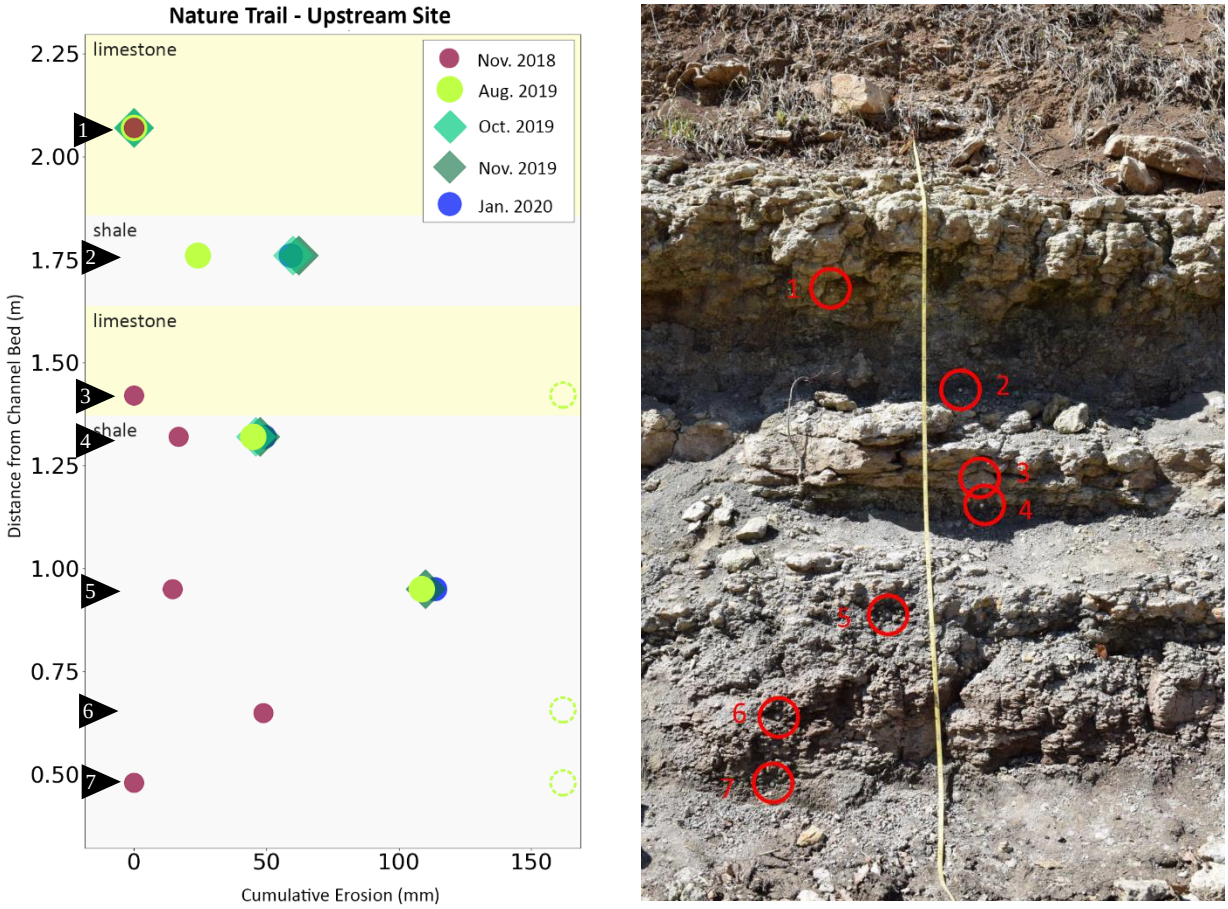

Figure 6.4 Measurement of cumulative erosion at each erosion pin at the upstream Nature Trail site since installment in April 2018. The hollow shape and color indicate the month that the pin went missing. The red circles and number correspond to the pin number in the black triangle on the y-axis of the graph.Erosion pins were not measured here in May 2019 because of a high water stage and discharge.

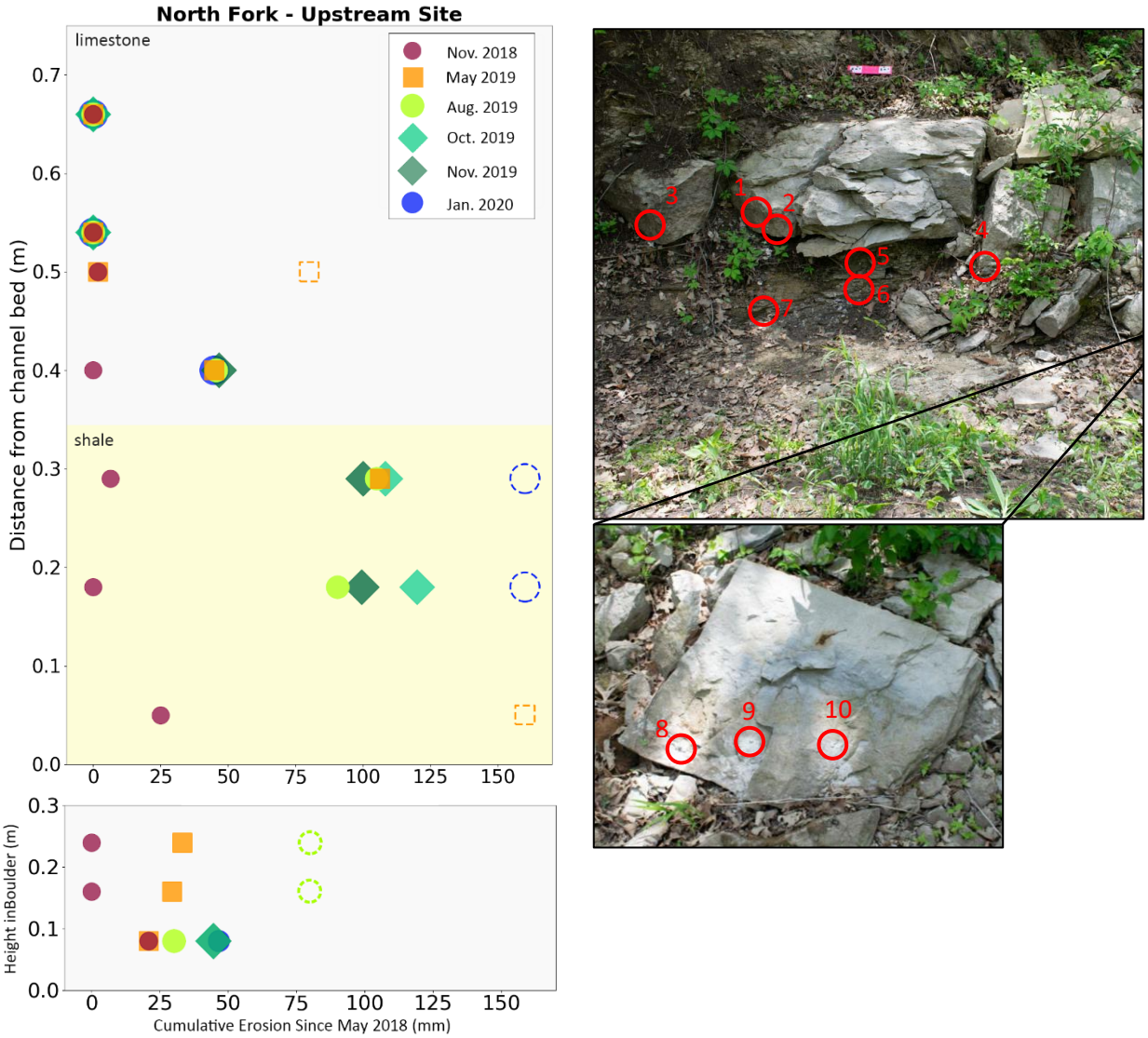

Figure 6.5 Measurement of cumulative erosion at each erosion pin at the upstream North Fork site since installment in April 2018. The lower portion of the graph are erosion pin measurements for the in-stream boulder (bottom right image) with pins 8, 9, and 10. The hollow shape and color indicate the month that the pin went missing. The red circles and number correspond to the pin number in the black triangle on the y-axis of the graph.

6.2 Structure from Motion

Three time slices from Nature Trail and North Fork downstream site were selected among those surveyed with SfM to compare spatial and temporal differences of deposition and erosion using Multi Scale Model to Model Cloud Compare (hereafter, M3C2) in CloudCompare. The time slices were April/May 2018 to May 2019 to capture a one-year duration from the start of the project, and May 2019 to October 2019 to capture the effects of the high flow events over the summer of 2019. Table 6.4 gives the survey and processing information in Agistoft Photoscan for each photoset.

Table 6.2 Processing and output information in from each photoset in Agisoft. The GCP error is the distance between the input and estimated positions of the markers. The tie point reprojection error is the averaged error of the distance between the point on the image and the original projection on the 3D dense point cloud.

Site	Survey date	# of photos	# of GCPs	Average GCP error	Tie Point Reprojection error (RMSE)	# of Points in Dense Cloud
North Fork	May 16, 2018	288	6	0.0007	1.06/pixel	26,623,047
	May 19, 2019	509	10	0.0006	0.94/pixel	13,523,994
	October 6, 2019	355	10	0.0006	0.90/pixel	19,325,250
Nature Trail	April 26, 2018	594	4	0.008	0.73/pixel	20,894,947
	May 22, 2019	603	8	0.0007	0.84/pixel	15,551,004
	October 27, 2019	495	8	0.0003	1.23/pixel	12,636,882

6.2.1 North Fork

The M3C2 output for the North Fork downstream site from May 2018 to May 2019 is shown in Figure 6.6. The red colored area, indicating deposition, is the large limestone boulder in the bank, which collapsed into the stream on December 23, 2018 (Figure A1). The limestone layer immediately to the right also collapsed into the stream, which is evident in the M3C2 output, as its former location is blue (for 'erosion') and its new position in the stream channel is red. The limestone boulder in stream on the bottom left of all frames gets slightly fractured and a piece gets plucked during this time period; however, this is not captured in the M3C2 output.

The M3C2 output for North Fork from May 2019 to October 2019 is shown in Figure 6.7. On the left side of the May 2019 image, there are boulders present that were transported away by the time of the October 2019 survey (as shown in light blue, ~70 cm of difference). This is also true of the large cobbles present under the tree trunk in May 2019. The cobbles circled in red

could be the cobbles that got displaced from the bank, or they could be new sediment that was transported and deposited from an upstream location. Again, M3C2 outputs do not capture the pieces of the in-stream limestone boulders that were plucked away. However, it is successful in capturing locations of large-scale sediment transport and deposition.

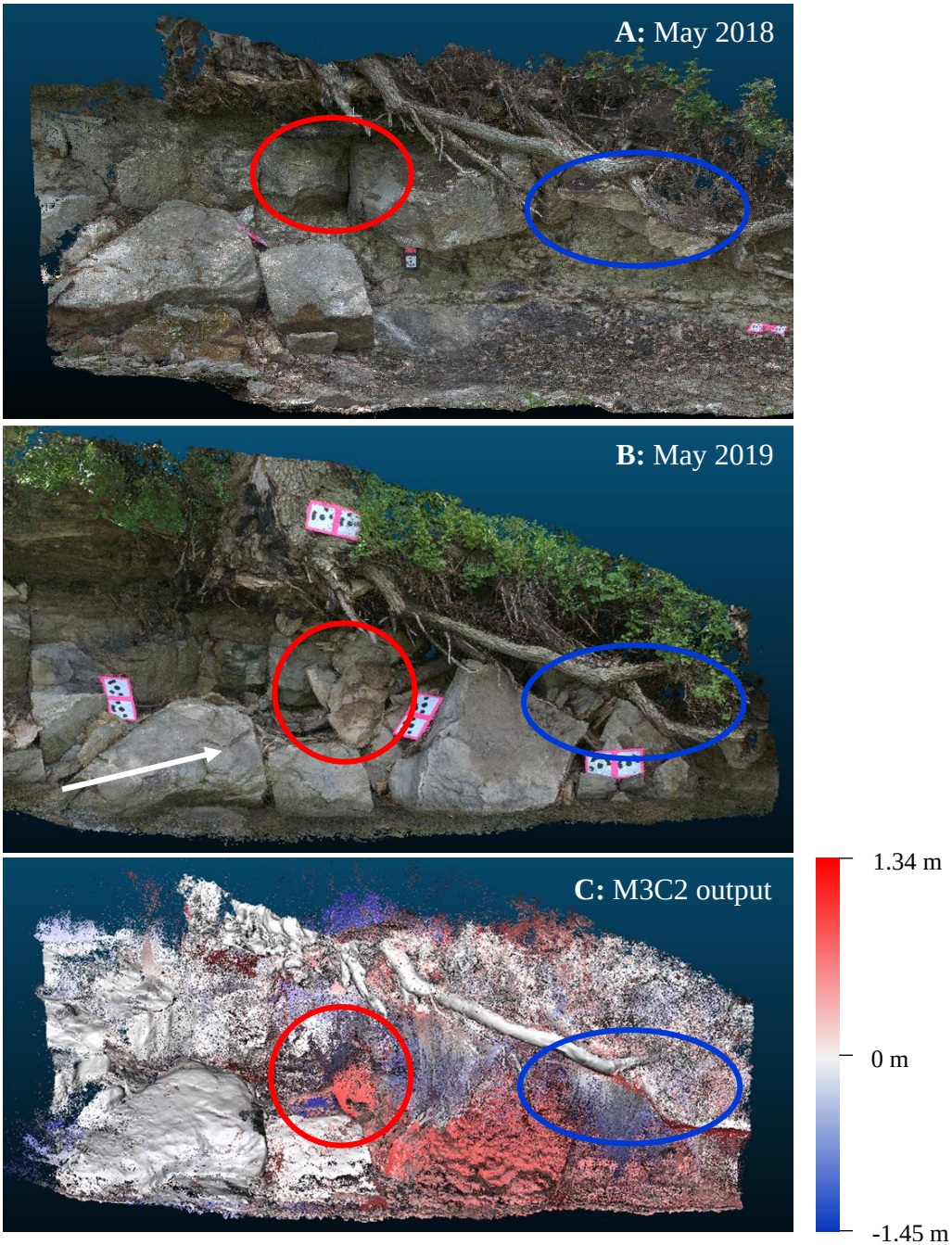

Figure 6.6 Downstream North Fork site; (A) May 2018 dense point cloud; (B) May 2019 dense point cloud. The white arrow indicates a piece that was plucked away but not captured by M3C2; (C) May 2018 to May 2019 M3C2 Output. Red is deposition and blue is erosion.

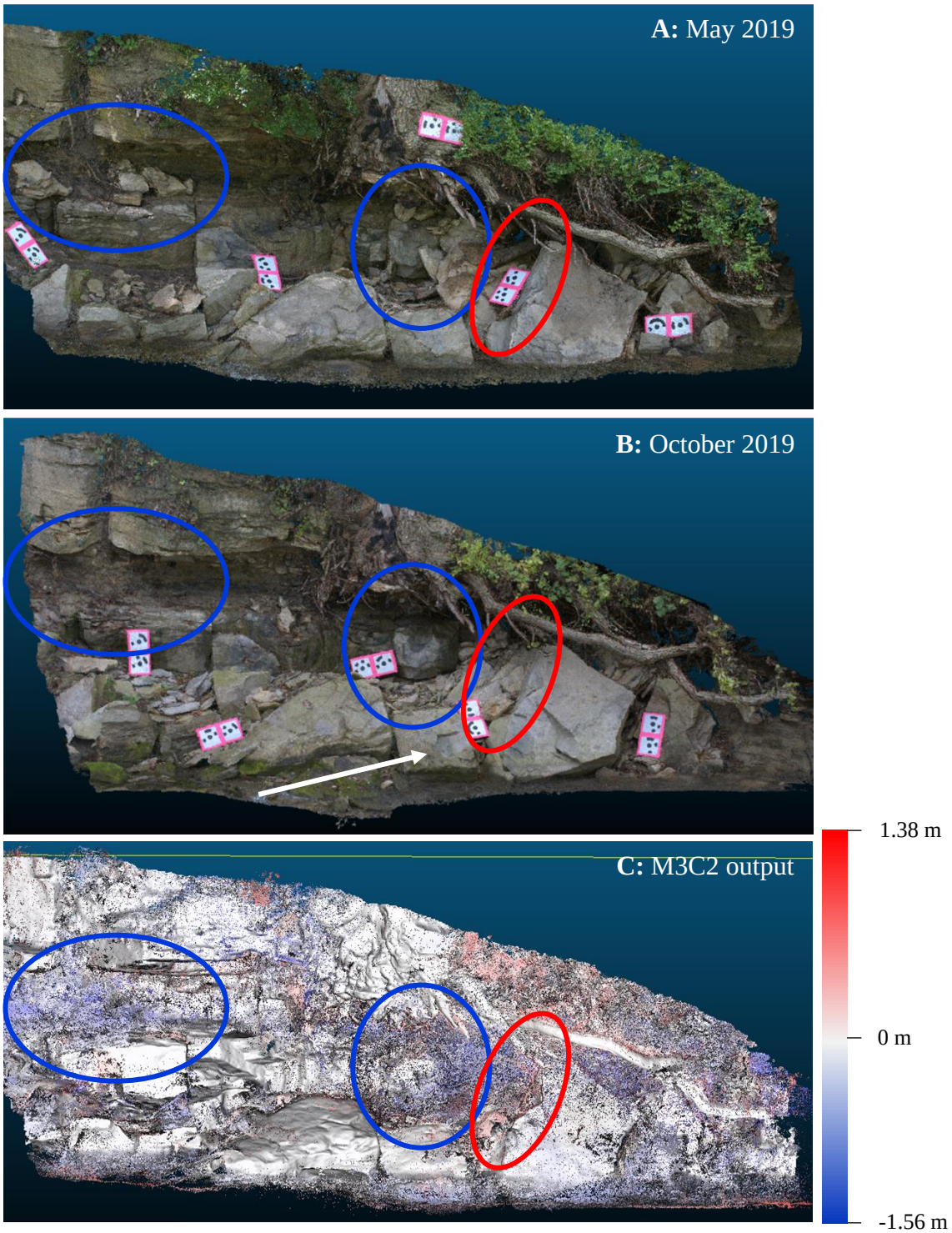

Figure 6.7 Downstream North Fork site; (A) May 2019 dense point cloud; (B) October 2019 dense point cloud. The white arrow indicates a piece that was plucked away but not captured by M3C2; (C) May 2019 to October M3C2 Output. Red is deposition and blue is erosion. On the far left is ~0.7m of erosion.

6.2.2 Nature Trail

The Nature Trail M3C2 output of April 2018 to May 2019 (Figure 6.8) captures erosion of the shale layers (in light blue), where as the limestone layers remain white, indicating that there was no erosion. The output also shows several locations where limestone blocks ~0.5 m in diameter have broken off from the channel bank. There is ~10 – 15 cm of erosion throughout much of the colluvium along the top half of the bank. At the top of the bank, there are spots of up to 25 cm of deposition, which may be due to hillslope runoff or slumping of the soil. In the top left corner, there is significant erosion, but it is difficult to say if this is the true amount of erosion or an artefact of the shadow from a nearby tree. The May 2019 to October 2019 output (Figure 6.9) show similar results; however, there are few limestone blocks that broke off from the bank and erosion in the colluvium appears to be less continuous and intense compared to the April 2018 to May 2019 one-year time slice (Figure 6.8). During this time period, much of the bank at the Nature Trail site was underwater, which disrupted SfM surveys.

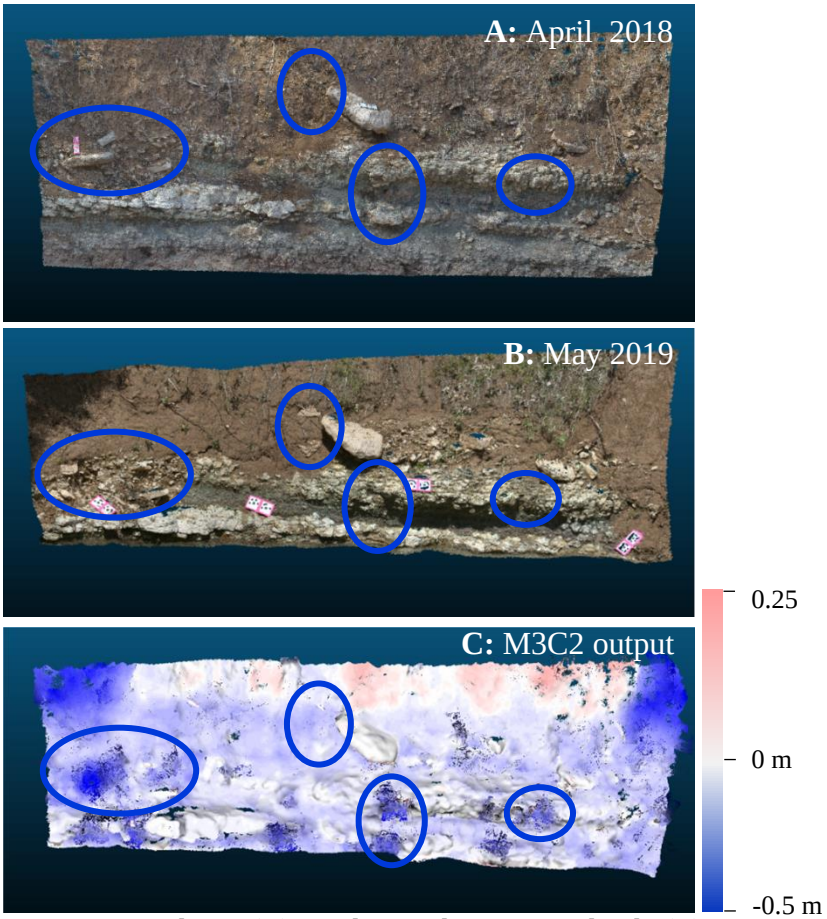

Figure 6.8 Nature Trail site; (A) April 2018 dense point cloud; (B) May 2019 dense point cloud. (C) May 2018 to May 2019 M3C2 Output. Red is deposition and blue is erosion.

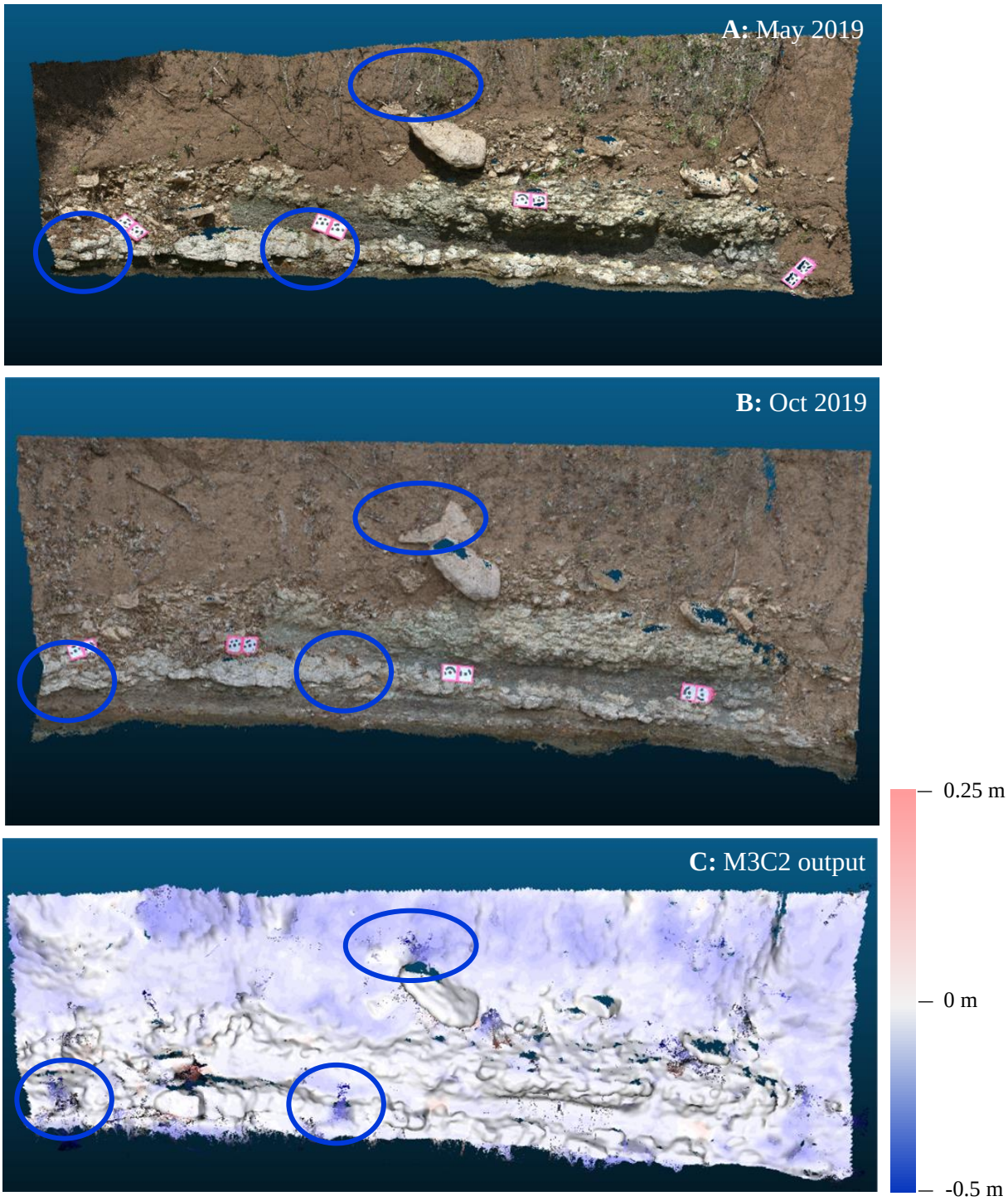

Figure 6.9 Nature Trail site; (A) May 2019 dense point cloud; (B) October 2019 dense point cloud. (C) May 2019 to October M3C2 Output. Red is deposition and blue is erosion.

Chapter 7 - Discussion

7.1 Modern Lateral Erosion Rates and Mechanisms

This study presents field measurements of lateral bedrock erosion. There are very few in situ measurements of bedrock erosion (e.g., Stock et al., 2005; Hartshorn et al., 2002; Collins et al., 2016; Beer et al., 2017), especially lateral erosion, as bedrock erosion rates are typically inferred from flights of strath terraces (Hancock et al., 1999; Brocard et al., 2003) or measured in experimental flume studies (Sklar & Dietrich, 2001; Carter & Anderson, 2006; Fuller et al., 2016).

Results show that substantial lateral erosion of shale and limestone occurred during the 21-month long study period. Erosion rates were higher than anticipated in both lithologies, especially in the limestone as it is a moderately strong lithology (Sklar & Dietrich, 2001). The measured limestone erosion rate in this study (20 mm/yr; section 6.1.2) is much higher than other reported limestone erosion rates (2.8 – 11.4 mm/yr; Brakenridge, 1985). Resistant lithologies, such as schist and granite, typically erode slowly, on the order of 0.3 – 5 mm/year (Whipple et al., 2000; Harsthorn et al., 2002; Brocard et al., 2003; Beer et al., 2017). In intermediate rocks, such as basalt and sandstone, mean erosion rates range from 6 – 100 mm/yr (Stock et al., 2005). Shale erosion rates reported in this study are 38.81 – 53.41 mm/yr (see section 6.1.1) . Shale and mudstone are weaker lithologies which typically erode on the order of 5 – 21 mm/year (Collins et al., 2016), but can be as high as 5 m/yr (Cook et al., 2014).

Erosion pin measurements and field observations indicate that plucking was the primary erosion mechanism in both limestone and shale lithologies. In shale bedrock, plucking is the most common erosion mechanism (e.g., Johnson & Finnegan, 2015); however, resistant lithologies, such as limestone, typically get eroded via abrasion (Whipple et al., 2013; Hartshorn et al., 2002). Because plucking was the primary erosion mechanism in both lithologies, this may contribute to substantially higher erosion rates, especially in the limestone layers, due to millimeters of erosion that occur via detachment of bedrock blocks that are lifted and transported away during flow events. The limestone bedrock in Konza may be weakened over time through weathering or abrasion by impacts from bedload particles (Figure 6.2), thus allowing loosely held pieces to be efficiently detached and transported by hydraulic forces. Dissolution of limestone was not observed during the study period; however, it may also contribute to the

weakening of the rock and make plucking more efficient (Krautblatter et al., 2012). In almost locations, pin installation was not observed to contribute to fracturing of the bedrock. However, in one instance, it is possible that installation of the erosion pin contributed to the fracturing of the limestone bedrock and may have made erosion via plucking more efficient (Pin #4, North Fork site). Additionally, measurements may be marginally over or underestimated due to difficulties measuring pins under deep water or microtopography of the bedrock surface, especially in limestone.

The highest amount of erosion occurred in both lithologies near the bottom of the banks and generally decreased with distance away from the channel bed (Figures 6.3, 4.4, 6.5; Tables 6.1, 6.2, and 6.3). Erosion is greater near the bed of the stream because there are more flow events capable of plucking bedrock, whereas locations increasing in height away from the channel bed receive fewer flow events and sediment impacts (Beer et al., 2017). Because erosion via plucking is the dominant erosion mechanism, the erosion rate depends on the frequency of events that exceed the threshold to detach and transport bedrock pieces (Snyder et al., 2003). Due to the slaking nature of shale, the threshold for plucking is much lower than in harder lithologies and even small flow events can sufficiently erode this bedrock. There was no measured erosion of the limestone pins installed in the stream banks at both sites. Rather, limestone erosion rates were highest on the in-stream slabs and boulders. This could be because they are protruding features or upstream facing and therefore receiving the most sediment impacts, and they are low in the channel and exposed to more flow events (e.g., Beer et al., 2017).

Rapid lateral erosion is occurring and is out-pacing vertical incision rates at the two study sites (Tables 6.1, 6.2, and 6.3). The rapid rates that I measured during this study may not be representative of long-term lateral erosion rates at theses reaches. The bedrock stream banks and bed are likely intermittently covered over decadal and centennial time scales. When bedrock is shielded by colluvium and fluvial deposits, bedrock erosion rates go to zero. Additionally, fluvial bedrock rates effectively go to zero when there is no water flow, such as during a drought or if the channel avulses away from the current channel. Shale could be eroded in the absence of water because of subaerial processes or freeze thaw cycles (Anderson et al., 2012), but the magnitude of erosion from flow events is likely much greater.

I observed the collapse of a large limestone block overlying shale bedrock at the North Fork downstream site, which protected the shale bedrock bank from erosion (Figure 6.6). Large

blocks with resistant lithology that collapse into the stream will effectively shut down lateral erosion on the valley wall, but not the collapsed block, because the bedrock banks are protected from hydraulic and sediment impacts by the collapsed material (Langston and Temme, 2019a). It is likely that continued rapid erosion of the shale at the North Fork upstream site will completely undercut the bank and cause additional limestone blocks to collapse into the stream, shielding the bank from continued rapid erosion. This is possible at the Nature Trail site; however, the limestone blocks that detached from the channel bank at Nature Trail during this study were smaller and more rapidly transported by the stream (Figure 6.8). Additionally, the limestone layers at the Nature Trail site are thinner and may not provide as extensive coverage of the bank as the limestone blocks at the North Fork site.

7.2 Structure from Motion

SfM was intended to supplement erosion pin measurements and give a meter-scale visualization of erosion and deposition at each site. SfM could not be used to supplement erosion pin measurements at the North Fork site because of the collapsed limestone boulder (Figure 6.6), and due to water covering the pins at the Nature Trail site for the duration of the study. The presence of water introduces error to surveys because of ripples and sun reflection that limit the ability of SfM point matching to match points (Cook, 2017). The water was not shallow enough to accurately match under water points, and therefore water points were removed from all dense point clouds before M3C2 processing.

Structure from motion successfully captured limestone block removal at both study sites (Figures 6.6 and 6.8), and transport and deposition of cobble-sized materials at the North Fork site (Figures 6.7 and 6.7). Individual block removal is qualitatively observed at the Nature Trail site; however, these appear as a cloud of dots rather than the shape of the blocks. This could be due to incorrect normals or projection scales used when calculating the M3C2 distance of two successive surveys (e.g., Crawford et al., 2018).

In addition to supplementing erosion pins, I expected that SfM could reveal plucking patterns in the limestone and shale. This was again limited by the water height at the Nature Trail site and by the limestone block covering the erosion pins at the North Fork site. The two instream limestone boulders at North Fork were fractured and pieces were plucked away. SfM could not resolve this, rather the rock surfaces in the M3C2 output appear to be smooth and the full depth of the limestone removal is not captured. The smoothing effect has been observed in

photogrammetric data to smooth over small-scale roughness, such as pebbles and boulders (Morgan et al., 2017) and rounding of large bedrock overhangs (Cook, 2017). The smoothing effect may contribute to loss of accuracy therefore limiting SfM's suitability in observing detailed changes (Cook, 2017; Jester & Klik, 2005). To reduce the smoothing effect, Cook (2017) advises an increase in quality parameter in Agisoft for the dense cloud construction. It is also likely that an increase in number of photos and photo coverage will increase the point cloud quality (i.e., Piermattei et al., 2015). However, homogenous surfaces such as limestone blocks or similar colored lithology are difficult to automatically match and the texture of the surface may not be fully captured, even at close range (Micheletti et al., 2015; Fonstad et al., 2013) Additionally, increasing the quality of the dense point cloud increases processing time considerably, and more noise can be introduced in a higher resolution point cloud (Cook, 2017). Micheletti et al. (2015) also noted that an increase in number of images may not linearly increase the model quality. The number of images required to capture the surface is instead site specific, and distribution of photo locations (i.e., camera angle) and sufficient photo overlap contribute to higher point cloud resolution (Dietrich, 2016; Fonstad et al., 2013)

For this study, I experimented with several variations of different processing parameters in Agisoft Photoscan and CloudCompare to determine the appropriate workflow for my study sites that best optimize processing time and output quality. A detailed sensitivity analysis of parameters for SfM processing and M3C2 is beyond the scope of this study, and therefore the advice of literature and software user manuals were considered as guides when determining the best workflow for my study. Erosion pins measurements at each of the transects were useful in this study to capture the spatio-temporal variability of erosion in the limestone and shale lithology sequences. SfM can be a powerful tool for monitoring erosion especially in alluvial settings (i.e., Prosdocimi et al., 2015; Marteau et al. 2017; Jugie et al., 2018). In my study, however, I found that SfM had less utility compared to erosion pin measurements and trail camera observations. This was likely due to the high water level at the Nature Trail site and the large collapse of blocks into the stream at the North Fork site, as well as the smoothing. SfM should therefore be used with caution.

7.3 Optically Stimulated Luminescence

OSL ages reported herein (Table 5.3) represent the depositional ages of preserved fluvial sediment that cap a strath terrace at the study reach. These ages represent a channel that

experienced periods of aggradation and channel migration during the late Pleistocene. The sediments throughout the OSL sampling transect appear to be well-preserved and not disturbed by roots or bioturbation, suggesting that post-depositional mixing that could introduce younger material is likely not a problem. However, the overdispersion and dose distribution of the samples (Figure 5.2) may indicate that some grains were partially bleached during sediment transport (Olley et al., 2004; Gray et al., 2017).

7.3.1 Regional Comparison

The OSL ages in this thesis are the oldest ages of fluvial terrace material reported for Kings Creek at Konza Prairie (Smith, 1991; Ross, 1995). Many previous studies in Northeast Kansas report fluvial material that is no older than Holocene in age (Johnson & Martin, 1987; Mandel, 2008). In the headwaters of Kings Creek, ~3000 meters upstream of the OSL sampling site of this thesis, Ross (1995) reported three radiocarbon ages of soil humates which were all ~2000 yr BP, and a charcoal fragment from a stratigraphically lower terrace yielded an age of 180 ± 80 yr BP. Smith (1991) reported radiocarbon ages of charcoal fragments sourced from two different fill terraces from a location ~1500 meters downstream from the OSL sampling location. The stratigraphically highest terrace, lying 2.9 to 6.4 m above the current channel, yielded an age of 8920 ± 120 yr BP (Figure 3.3B; Smith, 1991). The lower terrace, 2 to 5.9 m above the modern channel, yielded and age of 1770 ± 80 yr BP (Figure 3.3B; Smith, 1991). Smith (1991) also made a comprehensive map and correlated different terrace elevations to each other based on sedimentary structures, lithologies, textures, and terraces heights above the channel (Figure 3.3B). These radiocarbon ages correlate well with previous work establishing fluvial chronologies and stream behavior in the central Great Plains during the Holocene (e.g., Johnson and Martin, 1987 and references therein). Smith (1991) noted, however, that classifying terraces solely based on elevation and composition are not to best criteria to correlate stream terraces to one another. Therefore, more ages of fluvial terraces in Kings Creek are needed to define the fluvial history of Kings Creek, especially considering the results of this study that found depositional age as old as 36 ky.

7.3.2 Conceptual Valley Evolution

The fluvial material used for OSL dating is interpreted as floodplain material because it is fine-grained material interbedded with coarse grained cobble material. This indicates that the stream channel had to have been active at a lower elevation or different location in the valley

while maintaining channel-floodplain connectivity in order to overtop its banks during a high flow event and deposit fine material. The floodplain material is capped by layers of imbricated fluvial deposits of gravely and cobble-sized material, which means that the bed of the stream was at the elevation of the cobble layer when this sediment was deposited. The sediments throughout the OSL sampling transect appear to be well-preserved and not disturbed by roots or bioturbation, suggesting that post-depositional mixing that could introduce younger material is likely not a problem.

Figure 7.1 is a conceptual interpretation of the evolution of this valley as a cross section view. From the initial bedrock channel where the channel occupies all of the valley and is bounded by bedrock hillslopes (Figure 7.1A), Kings Creek must have undergone a period in the past where lateral erosion outpaced vertical incision to become a wide valley with bedrock sides that it is today (Figure 7.1B). The timing of periods of widening and lateral bedrock erosion is unknown with our current data, but lateral beveling of the bedrock surface that KNZ003 sits on must have been finished before KNZ003 was deposited (Figure 7.1C). The sample KNZ003 rests on a layer of cobble size material 25 cm above shale bedrock. The OSL age of KNZ003 indicates the last time the stream was active on this beveled bedrock surface, but the depositional age of KNZ003 does not necessarily indicate the time when this bedrock surface was cut laterally. Samples KNZ003 and KNZ004, 80 cm apart, are similar in age (30.8 ± 4.8 ka and 36.64 ± 4.36 ka, respectively) but do not fall in the expected chronological order (i.e., KNZ004 is stratigraphically higher but is “older” than KNZ003). However, the two sample ages overlap given the error and are therefore considered the same age, although the KNZ003 deposit must be older than KNZ004 given the law of superposition. This indicates that deposition in this area was very rapid when KNZ003 and KNZ004 were deposited. There is a layer of cobbley material separating KNZ003 and -004 (Figure 7.1D), indicating that the stream was laterally mobile during this period of rapid aggradation. The cobbley material was likely transported as bedload and deposited in or near the channel. The KNZ003 and -004 layers are floodplain material (Figure 7.1E) that were deposited when the channel was ~5 m away from active channel based on the observation of current floodplains.

The ages of KNZ004 and KNZ005, 50 cm from each other, have a larger age range (36.64 ± 4.36 ka and 19.91 ± 3.67 ka) and indicate that deposition rate at this site slowed during this time (Figure 7.1F). The channel may have migrated a significant distance southward from the sampling location, accounting for the ~15 ky period of time with no stream deposition in this

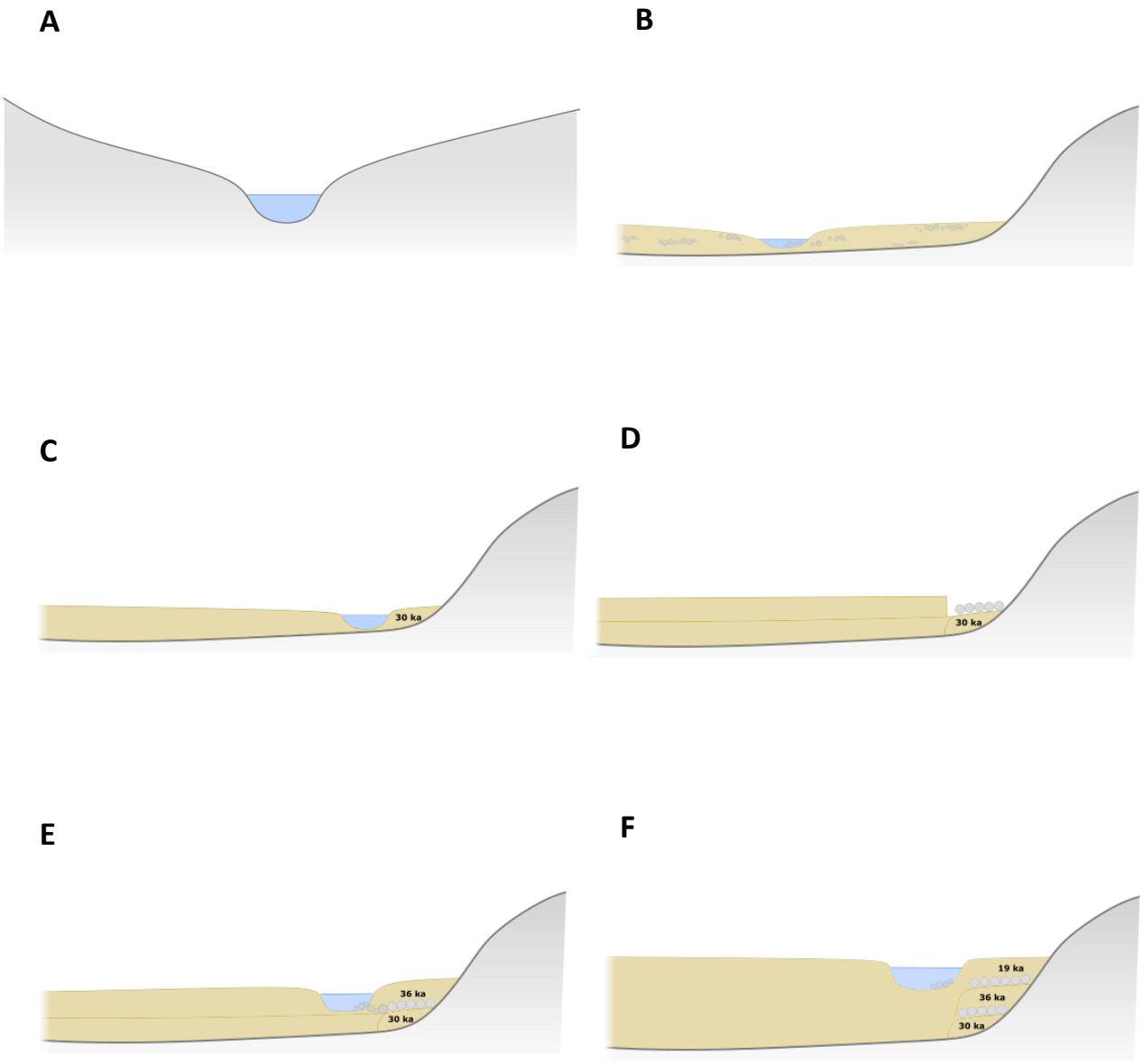

Figure 7.1 Conceptual interpretation of the evolution of the valley at the OSL sampling location. (A) Initial bedrock channel, prior to widening; (B) Kings Creek channel after a period of channel widening; (C) Deposition of KNZ003 (age 30 ka); (D) Deposition of the cobbly layer immediately above KNZ003. Channel aggradation and migration of Kings Creek away from the north side of the valley; (E) Kings Creek returning to the north side of the valley and depositing KNZ004 (age 36 ka); (F) After a ~15 ky depositional hiatus, Kings Creek has aggraded and deposited KNZ005 (age 19 ka).

location. While the stream was not depositing at the OSL sampling site, it could have spent that time aggrading and filling up the valley with fluvial sediment further south. KNZ001 and KNZ005 are similar in age and lie at roughly the same elevation above bedrock (1.55 – 1.7m), which reinforces confidence in the accuracy of OSL dating method. This suggests that ~19,000 years ago, KNZ001 and KNZ005 were at the elevations of floodplains being deposited on top of a bedrock surface roughly 1 m below. There is a final cobble layer above the KNZ005 sampling layer, thus the stream was active at a higher elevation after ~19 ka. Sometime after 19 ka, the valley was filled to ~4.5 m above the current channel with fluvial material as a result of an actively aggrading stream (Figure 7.1G). Mandel (2008) suggests that streams were aggrading

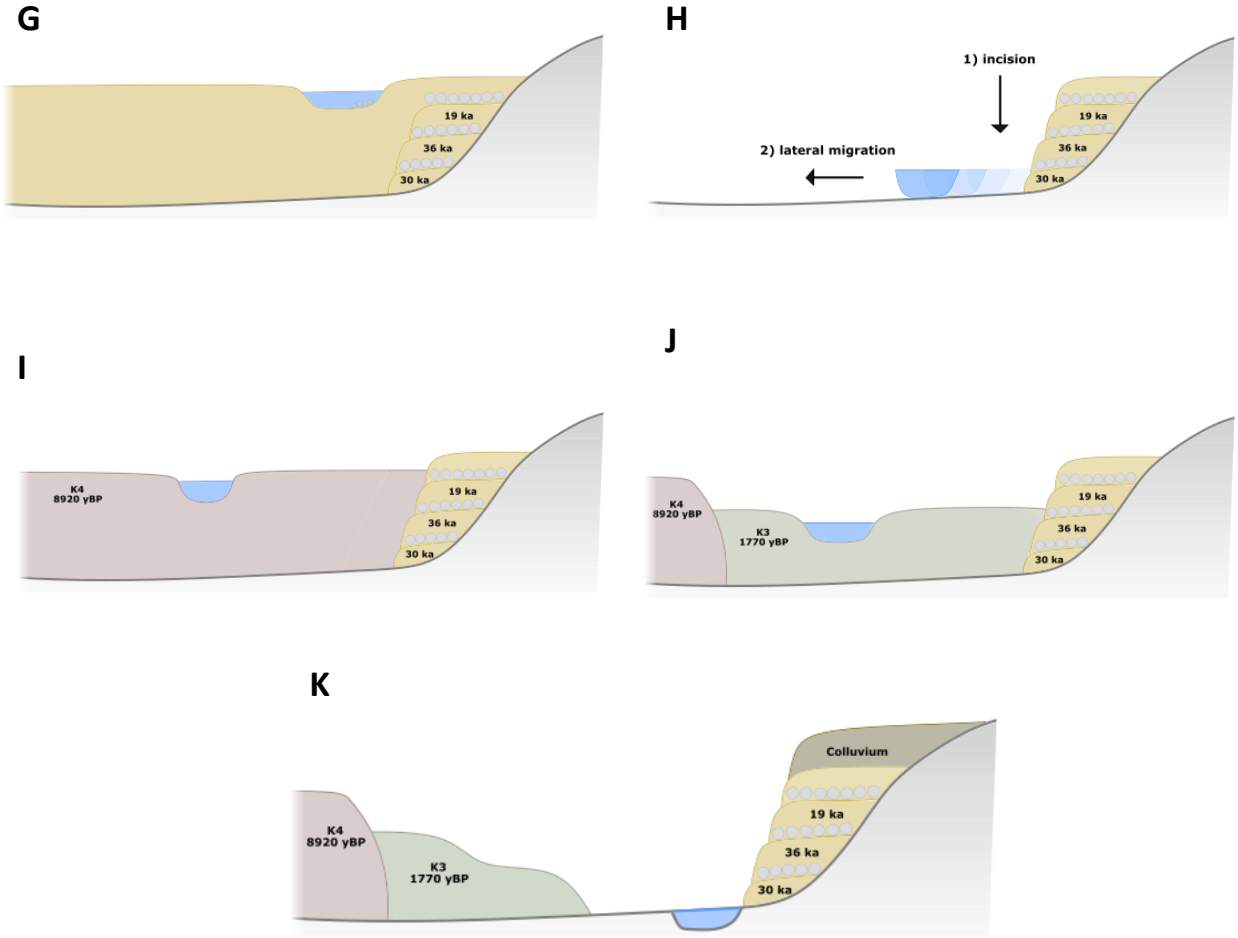

Figure 7.1 continued: (G) Sometime after 19 ky, Kings Creek was filled to ~4.5m above the current channel as a result of an actively aggrading stream; (H) Kings Creek incised into the alluvial fill sequence; (I) Valley filled with reworked loess by ~9 ky to create the K4 terrace (Smith, 1991); (J) A shift in stream behavior caused Kings Creek to incise then refill to create the K3 terrace (Smith, 1991); (K) Kings Creek then shifted behavior and experienced a period of downcutting to the modern stream elevation.

slowly enough that soil formation kept pace with river aggradation during the Pleistocene-Holocene boundary (~12 ka). Sometime after 19ka, Kings Creek incised into the alluvial fill sequence of KNZ003, 004, 005, and KNZ001 (Figure 7.1H). The exact timing of incision into the alluvial fill sequence is unknown but may have occurred ~8 – 5 ka when mid-continent storms brought intense, erosive rainstorms (Mandel, 2008).

Given the two fill terraces at Kings Creek dated by Smith (1991), it is necessary to reconcile OLS ages from this study with the radiocarbon ages found by Smith (1991) from a terrace of similar elevation downstream. It is possible that the valley filled with reworked loess by ~9 ky to create the K4 fill terrace (Figure7.1I; Smith, 1991). The K3 terrace, age ~2 ka (Smith, 1991), is a fill terrace with cut terraces in some areas (Figure 7.1J). Kings Creek then shifted behavior and experienced a period of downcutting to the modern stream elevation (Figure 7.1K).

The OSL ages reported herein and the conceptual model demonstrates the likelihood of multiple evolutionary time scales of Kings Creek terraces. Furthermore, this shows that terraces similar in sedimentary composition and elevation above the channel do not always share the same age (e.g., Foster et al., 2017), and in fact have the potential to be vastly different in age.

7.3.3 Controls on Kings Creek Behavior

Geomorphic changes of stream behavior are in response to climate change and intrinsic geomorphic stressors (e.g., Schumm, 1973). Streams aggrade when the ratio of sediment flux to water flux increases, thus limiting the stream's ability to effectively transport all material supplied to it (e.g., Bufe et al., 2017). Research suggest that aggradation often occurs during glacial intervals (Hancock et al., 1999; van den Berg, 1996; Molnar et al., 1994; Dühnforth et al., 2012), and all OSL ages reported in this study (Table 5.3) indicate that fluvial material was deposited during the Wisconsin glacial period and around the time of the onset of Northern Hemisphere deglaciation (~19 to 20 ka; Clark et al., 2009). Aggradation during glacial intervals could be a result of decreasing rainfall amount and intensity, which increases the sediment to water ratio. Kansas was generally cool and dry during glacial periods (Baker et al., 2009; Mandel et al., 2016), which could lead to stream aggradation. Another possible scenario for aggradation is the introduction of increased local hillslope material to the system (e.g., Wegmann and Pazzaglia, 2002). Hillslope material may be destabilized by during glacial intervals due to increased frost-cracking and freeze thaw (Anderson et al., 2012). Increases in liberation of

sediment from hillslopes can also be attributed to climate-controlled changes in wildfire frequency and intensity (Pierce et al., 2004) or wildfire-induced debris flows and alluvial fan growth (Meyer et al., 1995). However, the tallgrass roots sufficiently bind the soil together below ground thus making extensive post-fire hillslope erosion unlikely at Konza (Larson et al., 2013; Veach et al., 2014). Therefore, both decreasing rainfall amount and hillslope sediment flux may be jointly responsible for aggradation of Kings Creek.

While top-down controls on water and sediment supply were possible drivers of aggradation in Kings Creek, base level control by the Kansas River also may have played a key role in aggradation. OSL and ^{14}C ages suggest that the Buck Creek Terrace of the Kansas River, 11 – 12 m above the modern floodplain (Sorenson et al., 1987), aggraded between 50 ka and 14 ka (Mandel et al., 2016) as part of the Severance Formation, a package of late Pleistocene alluvium and colluvium found in eastern Kansas and Nebraska river valleys (Layzell et al., 2017). Additionally, terrace fill from the North Fork of the Solomon river, tributary to the Kansas River, yields ^{14}C ages of 29.2 – 38.2 cal. yBP from buried soil (Johnson, 1993). OSL ages of 44.6 ka were reported from Smoky Hill River alluvium from ~13 – 16 m above the modern floodplain (Hanson et al., 2010). These terrace ages indicate that the Kansas River system was actively aggrading beginning at least ~50 ka. Climate modulated changes during the Pleistocene are reflected in the Kansas River (Johnson et al., 2019), and therefore in many tributary rivers and streams such as Kings Creek. Given that the Kansas River was 12 m or higher than its present elevation and the long period of aggradation in the Kansas River system, the Kansas River likely controlled aggradation and incision episodes in Kings Creek to some extent as its local base level during the late Pleistocene.

7.4 Linking Modern and Past Lateral Erosion

A river can occupy a terrace surface for many thousands of years before incising and abandoning the surface (e.g., Foster et al., 2017). As such, depositional ages of the alluvium capping strath terraces represent the minimum age that a strath surface was beveled (flattened by lateral erosion)(e.g., Li et al., 2013; Bufe et al., 2017; Foster et al., 2017). The OSL ages reported herein reflect the minimum beveling age, as well as a maximum estimate for the time the bedrock surface and terrace were last occupied at the sampling location.

The underlying bedrock surface was beveled through lateral bedrock erosion, and research suggests that the duration of time a river spends beveling a bedrock surface and

widening its valley is much longer than the time spent incising bedrock (Bufe et al., 2017; Foster et al., 2017; Dühnforth et al., 2012). While we cannot know the exact duration of lateral beveling of the Kings Creek valley from data presented herein, the modern lateral erosion rates reported within can provide an estimate of how long it may have taken to carve this bedrock valley and time spent beveling the bedrock surface. This is achieved by dividing the measured modern lateral erosion rates from the width of the modern valley ~450 m. Given the modern lateral erosion rates determined from this study and assuming lateral erosion occurs at the modern rate measured during this study continuously, the minimum time spent laterally widening the Kings Creek Valley would be 9,451 years if the bedrock banks were made entirely of shale. If the bedrock banks are made only of limestone, minimum time widening valley would be 21,614 years. The actual time spent widening would likely fall within the ranges of the two lithologies given that erosion rates in layered landscapes are complex and vary greatly in space and time (Perne et al., 2017).

The areal planation equation in Bufe et al. (2017) provides a means to determine the rate of fluvial planation of a bedrock surface. The equation states that how quickly an area was beveled is equal to that area, divided by the amount of time spent beveling the area. In order to arrive at a long-term lateral erosion rate and determine the duration of time the Kings Creek spent beveling the valley, dates from terraces both sides of the valley are needed. Making a direct comparison between modern lateral erosion rates and long-term lateral erosion and valley widening rates would also require an additional age of sediments capping bedrock on the south side of the Kings Creek valley.

Furthermore, additional ages across a transect of a beveled bedrock surface would shed light on when the stream was active on the bedrock surface within the valley. If two or more depositional ages are obtained from the bedrock surface and the neighboring straths, the duration of terrace occupation and a minimum time of how long it took to bevel the bedrock surface can be calculated. The OSL ages on the north side of the valley at Kings Creek provide the first half of a data set that could yield time spent beveling the bedrock valley, and thus set the stage for future work.

Chapter 8 - Conclusion

This study successfully measured annual rates of lateral bedrock erosion and identified dominant erosion mechanisms in a natural setting -- Kings Creek in northeast Kansas. Few studies suggest specific mechanisms or field measured rates of lateral bedrock erosion (e.g., Stock et al., 2005; Collins et al., 2016; Beer et al. 2017). Lateral erosion rates of limestone during this study averaged 20.82 mm/year and shale lateral erosion rates ranged from 38.81 – 53.41 mm/year. Based on these findings, rapid lateral erosion rates of both the shale and limestone lithologies over the study period occurred likely as a result of several high flow events during Summer 2019 that were capable of plucking bedrock pieces from the bank. *In situ* lateral erosion rates and physical mechanisms of lateral erosion from Kings Creek can be used in future work to help evaluate bridge foundations and their vulnerability to scour and flood damage (e.g., Kattell & Eriksson, 1998). These field measured annual lateral erosion rates can also inform landscape evolution models (e.g., Langston & Tucker, 2018), further expanding our understanding of how bedrock rivers erode laterally over time to carve wide bedrock valleys and form strath terraces.

Additionally, there is little information available about the rates of past processes in Kings Creek. OSL ages reported herein of fluvial deposits sourced from the strath terrace are older than any material dated in Konza, and thus set the stage to continue establishing a robust chronology for Kings Creek. The OSL ages from this study indicate that Kings Creek was actively aggrading and incising throughout the late Pleistocene. These data have the potential to aid in interpreting climate patterns of the late Pleistocene, and how a changing climate influences the timing of aggradation and incision cycles in Kings Creek. Identifying the drivers of present and past change is essential to predict how climate will continue to influence river behavior and shape landscapes in the future.

References

AgiSoft PhotoScan Professional (Version 1.2.6) (Software). (2018). Retrieved from: http://www.agisoft.com/downloads/installer/

Anderson, R. S., Anderson, S. P., & Tucker, G. E. (2012). Rock damage and regolith transport by frost: An example of climate modulation of the geomorphology of the critical zone. *Earth Surface Processes and Landforms*, *38*(3), 299–316. doi:10.1002/esp.3330

Arnold, L. J., Demuro, M., & Ruiz, M. N. (2012). Empirical insights into multi-grain averaging effects from "pseudo" single-grain OSL measurements. *Radiation Measurements*, *47*(9), 652–658. doi:10.1016/j.radmeas.2012.02.005

Attal, M., & Lavé, J. (2009). Pebble abrasion during fluvial transport: Experimental results and implications for the evolution of the sediment load along rivers. *Journal of Geophysical Research: Earth Surface*, *114*(4), 1–23. doi:10.1029/2009JF001328

Baker, R.G., Bettis III, E.A., Mandel, R.D., Dorale, J.A., Fredlund, G.G, (2009). Mid-Wisconsinan environments on the eastern Great Plains. *Quat. Sci. Rev. 28*, 873–889.

Baynes, E. R. C., Attal, M., Niedermann, S., Kirstein, L. A., Dugmore, A. J., & Naylor, M. (2015). Erosion during extreme flood events dominates holocene canyon evolution in northeast iceland. *Proceedings of the National Academy of Sciences of the United States of America*, *112*(8), 2355–2360. doi:10.1073/pnas.1415443112

Beer, A. R., Turowski, J. M., & Kirchner, J. W. (2017). Spatial patterns of erosion in a bedrock gorge. *Journal of Geophysical Research: Earth Surface*, *122*, 191–214. doi:10.1002/2016JF003850

Blair, J. M. 2019. ANA01 Weekly, seasonal and annual measurement of precipitation volume and chemistry collected as part of the National Atmospheric Deposition Program at Konza Prairie . Environmental Data Initiative. doi:10.6073/pasta/6759f366220e482e181330e2c0947a2c

Brakenridge, R. G. (1985). Rate estimates for lateral bedrock erosion based on radiocarbon ages, Duck River, Tennessee. *Geology*, *13*(2), 111–114.

Brocard, G. Y., van der Beek, P. A., Bourlès, D. L., Siame, L. L., & Mugnier, J. L. (2003). Long-term fluvial incision rates and postglacial river relaxation time in the French Western Alps from 10Be dating of alluvial terraces with assessment of inheritance, soil development and wind ablation effects. *Earth and Planetary Science Letters*, *209*(1–2), 197–214. doi:10.1016/S0012-821X(03)00031-1

Bufe, A., Paola, C., & Burbank, D. W. (2016). Fluvial beveling of topography controlled by lateral channel mobility and uplift rate. *Nature Geoscience*, *9*(9), 706–710. doi:10.1038/ngeo2773

Bufe, A., Burbank, D. W., Liu, L., Bookhagen, B., Qin, J., Chen, J., … Yan, H. (2017). Variations of Lateral Bedrock Erosion Rates Control Planation of Uplifting Folds in the Foreland of the Tian Shan, NW China. *Journal of Geophysical Research: Earth Surface*, *122*, 2431–2467. doi:10.1002/2016JF004099

Bull, W. B. (1990). Stream-terrace genesis: Implications for soil development, *Geomorphology*, *3*(3), 351–367. doi:10.1016/0169-555X(90)90011-E

Burbank, Douglas W., & Anderson, Robert S. (2011). Geomorphic Markers. In *Tectonic Geomorphology* (pp. 17-44). Chichester, UK: John Wiley & Sons

Burbank, D. W., Leland, J., Fielding, E., Anderson, R. S., Brozovic, N., Reid, M. R., & Duncan, C. (1996). Bedrock incision, rock uplift and threshold hillslopes in the northwestern Himalayas. *Nature*. doi:10.1038/379505a0

Carter, C. L., & Anderson, R. S. (2006). Fluvial erosion of physically modeled abrasion-dominated slot canyons. *Geomorphology*, *81*(1–2), 89–113. doi:10.1016/j.geomorph.2006.04.006

Clark, P. U., Dyke, A. S., Shakun, J. D., Carlson, A. E., Clark, J., Wohlfarth, B., … McCabe, A. M. (2009). The Last Glacial Maximum. *Science*, *325*(5941), 710–714. doi:10.1126/science.1172873

CloudCompare (version 2.10.2) [GPL software]. (2019). Retrieved from: http://www.cloudcompare.org/

Collins, B. D., Montgomery, D. R., Schanz, S. A., & Larsen, I. J. (2016). Rates and mechanisms of bedrock incision and strath terrace formation in a forested catchment, Cascade Range, Washington. *Bulletin of the Geological Society of America*, *128*(5–6), 926–943. doi:10.1130/B31340.1

Cook, K. L. (2017). An evaluation of the effectiveness of low-cost UAVs and structure from motion for geomorphic change detection. *Geomorphology*, *278*, 195–208. doi:10.1016/j.geomorph.2016.11.009

Cook, K. L., Turowski, J. M., & Hovius, N. (2014). River gorge eradication by downstream sweep erosion. *Nature Geoscience*, *7*(9), 682–686. doi:10.1038/ngeo2224

Costigan, K. H., Daniels, M. D., & Dodds, W. K. (2015). Fundamental spatial and temporal disconnections in the hydrology of an intermittent prairie headwater network. *Journal of Hydrology*, *522*, 305–316. doi:10.1016/j.jhydrol.2014.12.031

Couper, P. R., & Maddock, I. P. (2001). Subaerial river bank erosion processes and their interaction with other bank erosion mechanisms on the River Arrow, Warwickshire, UK. *Earth Surface Processes and Landforms*, *26*(6), 631–646. doi:10.1002/esp.212

Crawford, A. J., Mueller, D., & Joyal, G. (2018). Surveying drifting icebergs and ice islands: Deterioration detection and mass estimation with aerial photogrammetry and laser scanning. *Remote Sensing*, *10*(4). doi:10.3390/rs10040575

Crosby, B. T., & Whipple, K. X. (2006). Knickpoint initiation and distribution within fluvial networks: 236 waterfalls in the Waipaoa River, North Island, New Zealand. *Geomorphology*, *82*(1–2), 16–38. doi:10.1016/j.geomorph.2005.08.023

DeVecchio, D. E., Heermance, R. V., Fuchs, M., & Owen, L. A. (2012). Climate-controlled landscape evolution in the Western Transverse Ranges, California: Insights from Quaternary geochronology of the Saugus Formation and strath terrace flights. *Lithosphere*, *4*(2), 110–130. doi:10.1130/L176.1

Dietrich, J. T. (2016). Riverscape mapping with helicopter-based Structure-from-Motion photogrammetry. *Geomorphology*, *252*, 144–157. doi:10.1016/j.geomorph.2015.05.008

Dühnforth, M., Anderson, R. S., Ward, D. J., & Blum, A. (2012). Unsteady late Pleistocene incision of streams bounding the Colorado Front Range from measurements of meteoric and in situ 10Be. *Journal of Geophysical Research: Earth Surface*, *117*(1), 1–20. doi:10.1029/2011JF002232

Duller, G. A. T. (2004). Luminescence dating of Quaternary sediments: Recent advances. *Journal of Quaternary Science*, *19*(2), 183–192. doi:10.1002/jqs.809

Durcan, J. A., King, G. E., & Duller, G. A. T. (2015). DRAC: Dose Rate and Age Calculator for trapped charge dating. *Quaternary Geochronology*, *28*, 54–61. doi:10.1016/j.quageo.2015.03.012

Duró, G., Crosato, A., Kleinhans, M. G., & Uijttewaal, W. S. J. (2018). Bank erosion processes measured with UAV-SfM along complex banklines of a straight mid-sized river reach. *Earth Surface Dynamics*, *6*(4), 933–953. doi:10.5194/esurf-6-933-2018

Finnegan, N. J., & Dietrich, W. E. (2011). Episodic bedrock strath terrace formation due to meander migration and cutoff. *Geology*, *39*(2), 143–146. doi:10.1130/G31716.1

Fonstad, M. A., Dietrich, J. T., Courville, B. C., Jensen, J. L., & Carbonneau, P. E. (2013). Topographic structure from motion: A new development in photogrammetric measurement. *Earth Surface Processes and Landforms*, *38*(4), 421–430. doi:10.1002/esp.3366

Foster, M. A., Anderson, R. S., Gray, H. J., & Mahan, S. A. (2017). Dating of river terraces along Lefthand Creek, western High Plains, Colorado, reveals punctuated incision. *Geomorphology*, *295*(June), 176–190. doi:10.1016/j.geomorph.2017.04.044

Fuller, T. K., Gran, K. B., Sklar, L. S., & Paola, C. (2016). Lateral erosion in an experimental bedrock channel: The influence of bed roughness on erosion by bed load impacts. *Journal of Geophysical Research: Earth Surface, 121*, 1084–1105. doi:doi:10.1002/ 2015JF003728

Galbraith, R. F., & Roberts, R. G. (2012). Statistical aspects of equivalent dose and error calculation and display in OSL dating: An overview and some recommendations. *Quaternary Geochronology*, *11*, 1–27. doi:10.1016/j.quageo.2012.04.020

Gray, L. J, Macpherson, G. L., Koelliker, J. K., & Dodds, W. K. (1998). Hydrology and Aquatic Chemistry. In Knapp, A.K., Briggs, J.M., Hartnett, D.C., and Collins, S.L. (Eds.), *Grassland Dynamics: Long-Term Ecological Research in Tallgrass Prairie* (pp. 35-47). New York, New York: Oxford University Press, Inc.

Gray, H. J., Tucker, G. E., Mahan, S. A., McGuire, C., & Rhodes, E. J. (2017). On extracting sediment transport information from measurements of luminescence in river sediment. *Journal of Geophysical Research: Earth Surface*, *122*, 1–24. doi:10.1002/2016JF003858

Hancock, G. S., & Anderson, R. S. (2002). Numerical modeling of fluvial strath-terrace formation in response to oscillating climate. *Bulletin of the Geological Society of America*, *114*(9), 1131–1142. doi:10.1130/0016-7606(2002)114<1131:NMOFST>2.0.CO

Hancock, G. S., Anderson, R. S., Chadwick, O. A., & Finkel, R. C. (1999). Dating fluvial terraces with 10Be and 26Al profiles: Application to the Wind River, Wyoming. *Geomorphology*, *27*(1–2), 41–60. doi:10.1016/S0169-555X(98)00089-0

Hancock, G. S., Anderson, R. S., & Whipple, K. X. (1998). Beyond Power: Bedrock River Incision Processes and Form. In: Tinkler, K., Wohl, E.E. (Eds.), *Rivers Over Rock: Fluvial Processes in Bedrock Channels,* Geophysical Monograph Series, AGU Press, Washington, DC, volume 107, pp. 35–60.

Hanson, P. R., Arbogast, A. F., Johnson, W. C., Joeckel, R. M., & Young, A. R. (2010). Megadroughts and late Holocene dune activation at the eastern margin of the Great Plains, north-central Kansas, USA. *Aeolian Research*, *1*(3–4), 101–110. doi:10.1016/j.aeolia.2009.10.002

Harden, C. P., Chartrand, K. J., & Henry, E. (2010). Temporal variability of bank erosion in East Tennessee headwater streams. *Southeastern Geographer*, *50*(4), 484–502.

Hartshorn, K., Hovius, N., Dade, W. B., & Slingerland, R. L. (2002). Climate-driven bedrock incision in an active mountain belt. *Science*, *297*(5589), 2036–2038. doi:10.1126/science.1075078

Hayden, B. P. (1998). Regional climate and the distribution of tallgrass prairie. In A. K. Knapp, J. M. Briggs, D. C. Hartnett & S. L. Collins (Eds.), *Grassland dynamics: long-term ecological research in tallgrass prairie* (pp. 19-34). New York: Oxford University Press.

Hooke, J. M. (1979). An analysis of the processes of river bank erosion. Journal of Hydrology, 42:39-62. doi:10.1016/0022-1694(79)90005-2

Javernick, L., Brasington, J., & Caruso, B. (2014). Modeling the topography of shallow braided rivers using Structure-from-Motion photogrammetry. *Geomorphology*, *213*, 166–182. doi:10.1016/j.geomorph.2014.01.006

Jester, W., & Klik, A. (2005). Soil surface roughness measurement - Methods, applicability, and surface representation. *Catena*, *64*(2–3), 174–192. doi:10.1016/j.catena.2005.08.005

Johnson, K. N., & Finnegan, N. J. (2015). A lithologic control on active meandering in bedrock channels. *Bulletin of the Geological Society of America*, *127*(11–12), 1766–1776. doi:10.1130/B31184.1

Johnson, W. C. (1993). *Surficial geology and stratigraphy of Phillips County, Kansas, with emphasis on the Quaternary Period*. Kansas Geological Survey.

Johnson, W. C. & Martin, C. W., (1987). Holocene alluvial stratigraphic studies from Kansas and adjoining states of the easte-central Plains. In Johnson, W. C., e.d, Quaternary Environments of Kansas: Kansas Geological Survey Guidebook, Series 5, p. 109-122.

Johnson, W. C., Halfen, A. F., Spencer, J. Q. G., Hanson, P. R., Mason, J. A., & Young, A. R. (2019). Late MIS 3 stabilization of dunes in the eastern Central Great Plains, USA. *Aeolian Research*, *36*(June 2018), 68–81. doi:10.1016/j.aeolia.2018.12.002

Jugie, M., Gob, F., Virmoux, C., Brunstein, D., Tamisier, V., Le Coeur, C., & Grancher, D. (2018). Characterizing and quantifying the discontinuous bank erosion of a small low energy river using Structure-from-Motion Photogrammetry and erosion pins. *Journal of Hydrology*, *563*(February), 418–434. doi:10.1016/j.jhydrol.2018.06.019

Kasse, C., Vandenberghe, D., De Corte, F., & Haute, Van den Haute, P. (2007). Late Weichselian fluvio-aeolian sands and coversands of the type locality Grubbenvorst (southern Netherlands): sedimentary environments, climate record and age. *Journal of Quaternary Science*, *22*(7), 695–708. doi:10.1002/jqs.1087

Kattell, J., & Eriksson, M. (1998). Bridge scour evaluation: screening, analysis, and countermeasures. General Technical Report 9877 1207–SDTDC, U.S. Department of Agriculture, Forest San Dimas, CA.

Keen-Zebert, A., Tooth, S., Rodnight, H., Duller, G. A. T., Roberts, H. M., & Grenfell, M. (2013). Late Quaternary floodplain reworking and the preservation of alluvial sedimentary archives in unconfined and confined river valleys in the eastern interior of South Africa. *Geomorphology*, *185*, 5

Knapp, A.K., Seastedt, T.R. (1998). Grasslands, Konza Prairie, and Long-Term Ecological Research. In Knapp, A.K., Briggs, J.M., Hartnett, D.C., and Collins, S.L. (Eds.), *Grassland*

Dynamics: Long-Term Ecological Research in Tallgrass Prairie (pp. 35-47). New York, New York: Oxford University Press, Inc

Krautblatter, M., M. Moser, L. Schrott, J. Wolf, & D. Morche. (2012). Significance of rockfall magnitude and carbonate dissolution for rock slope erosion and geomorphic work on alpine limestone cliffs (Reintal, German Alps). *Geomorphology, 167-168,* 21-34.

Kreutzer, S., Schmidt, C., Fuchs, M., Dietze, M., Fischer, M., & Fuchs, M. (2012). Introducing an R package for luminescence dating analysis. *Ancient TL*, *30*(1), 1–8.

Lague, D., Brodu, N., & Leroux, J. (2013). Accurate 3D comparison of complex topography with terrestrial laser scanner: Application to the Rangitikei canyon (N-Z). *ISPRS Journal of Photogrammetry and Remote Sensing*, *82*, 10–26. doi:10.1016/j.isprsjprs.2013.04.009

Lamb, M. P., Dietrich, W. E., & Sklar, L. S. (2008). A model for fluvial bedrock incision by impacting suspended and bed load sediment. *Journal of Geophysical Research: Earth Surface*, *113*(3), 1–18. doi:10.1029/2007JF000915

Lamb, M. P., Finnegan, N. J., Scheingross, J. S., & Sklar, L. S. (2015). New insights into the mechanics of fluvial bedrock erosion through flume experiments and theory. *Geomorphology*, *244*, 33–55. doi:10.1016/j.geomorph.2015.03.003

Lamb, M. P., & Fonstad, M. A. (2010). Rapid formation of a modern bedrock canyon by a single flood event. *Nature Geoscience*, *3*(7), 477–481. doi:10.1038/ngeo894

Langston, A. L., & Temme, A. J. A. M. (2019a). Impacts of Lithologically Controlled Mechanisms on Downstream Bedrock Valley Widening. *Geophysical Research Letters*, *46*(21), 12056–12064. doi:10.1029/2019GL085164

Langston, A. L., & Temme, A. J. A. M. (2019b). Bedrock erosion and changes in bed sediment lithology in response to an extreme flood event: The 2013 Colorado Front Range flood. *Geomorphology*, *328*, 1–14. doi:10.1016/j.geomorph.2018.11.015

Langston, A. L., & Tucker, G. E. (2018). Developing and exploring a theory for the lateral erosion of bedrock channels for use in landscape evolution models. *Earth Surface Dynamics*, *6*(1), 1–27. doi:10.5194/esurf-6-1-2018

Langston, A. L., Tucker, G. E., & Anderson, R. S. (2015). Interpreting climate-modulated processes of terrace development along the Colorado Front Range using a landscape evolution model. *Journal of Geophysical Research F: Earth Surface*, *120*(10), 2121–2138. doi:10.1002/2014JF003403

Larson, D. M., Grudzinski, B. P., Dodds, W. K., Daniels, M. D., Skibbe, A., & Joern, A. (2013b). Blazing and grazing: influences of fire and bison on tallgrass prairie stream water quality. *Freshwater Science*, *32*(3), 779–791. https://doi.org/10.1899/12-118.1

Lawler, D. M. (1993). The measurement of river bank erosion and lateral channel change: A review. *Earth Surface Processes and Landforms*, *18*, 777–821. doi:doi:10.1002/esp.3290180905

Layzell, A. L., Sawin, R. S., Mandel, R. D., Ludvigson, G. A., Franseen, E. K., West, R. R., & Lynn Watney, W. (2017). Quaternary stratigraphy and stratigraphic nomenclature revisions in Kansas. *Current Research in Earth Sciences*, *263*(November), 1–8.

Li, T., Chen, J., Thompson, J. A., Burbank, D. W., & Yang, X. (2013). Quantification of three-dimensional folding using fluvial terraces: A case study from the Mushi anticline, northern margin of the Chinese Pamir. *Journal of Geophysical Research: Solid Earth*, *118*(8), 4628–4647. doi:10.1002/jgrb.50316

Liritzis, I., Stamoulis, K., Papachristodoulou, C., & Ioannides, K. (2013). A re-evaluation of radiation dose-rate conversion factors. *Mediterr. Archaeol. Archaeom 13*, 1–15.

Macpherson, G. L. (1996). Hydrogeology of thin limestones: The Konza prairie long-term ecological research site, Northeastern Kansas. *Journal of Hydrology*, *186*(1–4), 191–228. doi:10.1016/S0022-1694(96)03029-6

Mandel, R. D. (2008). Buried paleoindian-age landscapes in stream valleys of the central plains, USA. *Geomorphology*, *101*(1–2), 342–361. doi:10.1016/j.geomorph.2008.05.031

Mandel, R. D., Bettis III, E. A., & Hanson, P. R. (2016). Characteristics and geochronology of the Severance Formation: a new mid- through late-Wisconsinan lithostratigraphic unit in the eastern plains of North America. Geological Society of America Abstracts with Programs 48 (7). doi:10.1130/abs/2016AM-286301

Marteau, B., Vericat, D., Gibbins, C., Batalla, R. J., & Green, D. R. (2017). Application of Structure-from-Motion photogrammetry to river restoration. *Earth Surface Processes and Landforms*, *42*(3), 503–515. doi:10.1002/esp.4086

Merritts, D. J., Vincent, K. R., & Wohl, E. E. (1994). Long river profiles, tectonism, and eustasy: A guide to interpreting fluvial terraces. *Journal of Geophysical Research*, *99*, 14031–14050.

Meyer, G. A., Wells, S. G., & Jull, A. J. T. (1995). Fire and alluvial chronology in Yellowstone National Park: climatic and intrinsic controls on Holocene geomorphic processes. *Geological Society of America Bulletin*, *107*(10), 1211–1230. doi:10.1130/0016-7606(1995)107<1211:FAACIY>2.3.CO;2

Micheletti, N., Chandler, J. H., & Lane, S. N. (2015). Investigating the geomorphological potential of freely available and accessible structure-from-motion photogrammetry using a smartphone. *Earth Surface Processes and Landforms*, *40*(4), 473–486. doi:10.1002/esp.3648

Molnar, P., Brown, E. T., Burchfiel, C., Qidong, D., Xianyue, F., Jun, L., … Huichauan, Y. (1994). Quaternary climate change and the formation of river terraces across growing anticlines on the north flank of the Tien Shan, China. *Journal of Geology*, *102*(5), 583–602. doi:10.1086/629700

Montgomery, D. R. (2004). Observations on the role of lithology in strath terrace formation and bedrock channel width. *American Journal of Science*, *304*, 454–476.

Montgomery, D. R., & Buffington, J. M. (1997). Channel-reach morphology in mountain drainage basins. *Bulletin of the Geological Society of America*, *109*(5):596–611. doi:10.1130/0016-7606(1997)109<0596:CRMIMD>2.3.CO;2

Montgomery, D. R., & Gran, K. B. (2001). Downstream variations in the width of bedrock channels. *Water Resources Research*, *37*(6), 1841–1846. doi:10.1029/2000WR900393

Morgan, J. A., Brogan, D. J., & Nelson, P. A. (2017). Application of Structure-from-Motion photogrammetry in laboratory flumes. *Geomorphology*, *276*, 125–143. doi:10.1016/j.geomorph.2016.10.021

Mosbrucker, A. R., Major, J. J., Spicer, K. R., & Pitlick, J. (2017). Camera system considerations for geomorphic applications of SfM photogrammetry. *Earth Surface Processes and Landforms*, *42*(6), 969–986. doi:10.1002/esp.4066

Mudd, S. M., & Furbish, D. J. (2007). Responses of soil-mantled hillslopes to transient channel incision rates. *Journal of Geophysical Research: Earth Surface*, *112*(3), 1–12. doi:10.1029/2006JF000516

Murray, A. S., & Olley, J. M. (2002). Stimulated Luminescence Dating of Sedimentary Quartz: A Status Review. *Journal of Methods and Applications of Absolue Chronology*, *21*, 1–16.

Murray, A. S., & Wintle, A. G. (2000). Luminescence dating of quartz using an improved single-aliquot regenerative-dose protocol. *Radiation Measurements*, *32*(1), 57–73. doi:10.1016/S1350-4487(99)00253-X

Nelson, M., Rittenour, T., & Cornachione, H. (2019). Sampling Methods for Luminescence Dating of Subsurface Deposits from Cores. *Methods and Protocols*, *2*(4), 88. doi:10.3390/mps2040088

Olley, J. M., Caitcheon, G. G., & Roberts, R. G. (1999). Origin of dose distributions in fluvial sediments, and the prospect of dating single grains from fluvial deposits using optically stimulated luminescence. *Radiation Measurements*, *30*(2), 207–217. doi:10.1016/S1350-4487(99)00040-2

Oviatt, C. G. (1998). Geomorphology of Konza Prairie. In Knapp, A.K., Briggs, J.M., Hartnett, D.C., and Collins, S.L. (Eds.), *Grassland Dynamics: Long-Term Ecological Research in Tallgrass Prairie* (pp. 35-47). New York, New York: Oxford University Press, Inc.

Pan, B., D. Burbank, Y. Wang, G. Wu, J. Li, and Q. Guan (2003). A 900 k.y. record of strath terrace formation during glacial-interglacial transitions in northwest China, *Geology, 31*(11), 957–960. doi:10.1130/G19685.1

Pazzaglia, F. J. (2013). *Fluvial Terraces*. *Treatise on Geomorphology* (Vol. 9). doi:10.1016/B978-0-12-374739-6.00248-7

Piermattei, L., Carturan, L., & Guarnieri, A. (2015). Use of terrestrial photogrammetry based on structure-from-motion for mass balance estimation of a small glacier in the Italian alps. *Earth Surface Processes and Landforms*, *40*(13), 1791–1802. doi:10.1002/esp.3756

Pierce, J. L., Meyer, G. A., & Jull, A. T. (2004). Fire-induced erosion and millennial-scale climate change in northern ponderosa pine forests. *Nature, 432*(7013):87–90.

Prescott, J. R., & Hutton, J. T. (1994). Cosmic ray contributions to dose rates for luminescence and ESR dating: large depths and long-term time variations. *Radiation measurements 23*, 497–500.

Prosdocimi, M., Calligaro, S., Sofia, G., Dalla Fontana, G., & Tarolli, P. (2015). Bank erosion in agricultural drainage networks: New challenges from structure-from-motion photogrammetry for post-event analysis. *Earth Surface Processes and Landforms*, *40*(14), 1891–1906. doi:10.1002/esp.3767

Rhodes, E. J. (2011). Optically Stimulated Luminescence Dating of Sediments over the Past 200,000 Years. *Annual Review of Earth and Planetary Sciences, 39*(1), 461–488. doi:10.1146/annurev-earth-040610-133425

Rittenour, T. M. (2008). Luminescence dating of fluvial deposits: Applications to geomorphic, palaeoseismic and archaeological research. *Boreas, 37*(4), 613–635. doi:10.1111/j.1502-3885.2008.00056.x

Roberts, R. G., Galbraith, R. F., Olley, J. M., Yoshida, H., & Laslett, G. M. (1999). Optical dating of single and multiple grains of quartz from Jinmium rock shelter, northern Australia: Part II, results and implications. *Archaeometry, 41*(2), 365–395. doi:10.1111/j.1475-4754.1999.tb00988.x

Roering, J. J., Kirchner, J. W., & Dietrich, W. E. (2001). Hillslope evolution by nonlinear, slope-dependent transport: Steady state morphology and equilibrium adjustment timescales. *Journal of Geophysical Research: Solid Earth*, *106*(B8), 16499–16513. doi:10.1029/2001jb000323

Ross, K. L. (1995). Geomorphology of the N4D watershed Konza Prairie Research Natural Area, Riley and Geary Counties, Kansas. Kansas State University Master's Thesis.

Rusnák, M., Sládek, J., Kidová, A., & Lehotský, M. (2018). Template for high-resolution river landscape mapping using UAV technology. *Measurement: Journal of the International*

Measurement Confederation, *115*(June 2017), 139–151. doi:10.1016/j.measurement.2017.10.023

Schanz, S. A., & Montgomery, D. R. (2016). Geomorphology Lithologic controls on valley width and strath terrace formation. *Geomorphology*, *258*, 58–68. doi:10.1016/j.geomorph.2016.01.015

Schumm, S. A. (1985). Patterns of Alluvial Rivers. *Annual Review of Earth and Planetary Sciences*, *13*, 5–27.

Schumm, S. A. (1973). Geomorphic Thresholds and Complex Response of Drainage Systems. In: Morisawa, M., (Ed.), Fluvial Geomorphology, Publications of Geomorphology, State University of New York, Binghamton, 299-310.

Sklar, L. S., & Dietrich, W. E. (2004). A mechanistic model for river incision into bedrock by saltating bed load. *Water Resources Research*, *40*(6), 1–22. doi:10.1029/2003WR002496

Sklar, L. S., & Dietrich, W. E. (2001). Sediment and rock strength controls on river incision into bedrock. *Geology*, *29*(12), 1087–1090. doi:10.1130/0091-7613(2001)029<1087:SARSCO>2.0.CO

Simon, A., Curini, A., Darby, S., & Langendoen, E. (1999). Streambank Mechanics and the role of bank and near-bank processes in incised channels. In: Stephen Darby and Andrew Simon (Eds.), *Incised River Channels: Processes, Forms, Engineering and Management*, John Wiley and Sons Ltd. Chichester. 442 p.

Smith, G. (1991). Geomorphology and Geomorphic History of the Konza Prairie Research Natural Area, Riley and Geary Counties, Kansas. Kansas State University Master's Thesis.

Snyder, N. P., Whipple, K. X., Tucker, G. E., & Merritts, D. J. (2003). Importance of a stochastic distribution of floods and erosion thresholds in the bedrock river incision problem. *Journal of Geophysical Research: Solid Earth*, *108*(B2). doi:10.1029/2001jb001655

Sorenson, C.J., Sallee, K.H., Mandel, R.D., (1987). Holocene and Pleistocene soils and geomorphic surfaces of the Kansas River valley. In: Johnson, W.C. (Ed.), Quaternary Environments of Kansas. Kansas Geological Survey Guidebook 5.

Spotila, J. A., Moskey, K. A., & Prince, P. S. (2015). Geologic controls on bedrock channel width in large, slowly-eroding catchments: Case study of the New River in eastern North America. *Geomorphology*, *230*, 51–63. doi:10.1016/j.geomorph.2014.11.004

Stock, J. D., Montgomery, D. R., Collins, B. D., Dietrich, W. E., & Sklar, L. (2005). Field measurements of incision rates following bedrock exposure: Implications for process controls on the long profiles of valleys cut by rivers and debris flows. *Bulletin of the Geological Society of America*, *117*(1–2), 174–194. doi:10.1130/B25560.1

Summa-Nelson, M. C., & Rittenour, T. M. (2012). Application of OSL dating to middle to late Holocene arroyo sediments in Kanab Creek, southern Utah, USA. *Quaternary Geochronology*, *10*, 167–174. doi:10.1016/j.quageo.2012.05.002

Tomkin, J. H., Brandon, M. T., Pazzaglia, F. J., Barbour, J. R., & Willett, S. D. (2003). Quantitative testing of bedrock incision models for the Clearwater River, NW Washington State. *Journal of Geophysical Research: Solid Earth*, *108*(B6). doi:10.1029/2001jb000862

Turowski, J. M., Hovius, N., Meng-Long, H., Lague, D., & Men-Chiang, C. (2008). Distribution of erosion across bedrock channels. *Earth Surface Processes and Landforms*, *33*,353–363. doi:10.1002/esp.1559

Van den Berg, M. W. (1996). *Fluvial sequences of the Maas, a 10 Ma record of neotectonics and climate change at various timescales*. Landbouwuniversiteit.

Veach, A. M., Dodds, W. K., & Skibbe, A. (2014). Fire and grazing influences on rates of riparian woody plant expansion along grassland streams. *PLoS ONE*, *9*(9), 1–9. Doi:10.1371/journal.pone.0106922

Vero, S. E., Macpherson, G. L., Sullivan, P. L., Brookfield, A. E., Nippert, J. B., Kirk, M. F., Datta, S., & Kempton, P. (2017). Developing a conceptual framework of landscape and hydrology on tallgrass prairie: A critical zone approach. *Vadose Zone Journal*. doi:10.2136/vzj2017.03.0069

Walker, M. (2005). *Quaternary Dating Methods.* John Wiley and Sons Ltd. West Sussex, England. Pp. 94-99.

Wegmann, K. W., & Pazzaglia, F. J. (2002). Holocene strath terraces, climate change, and active tectonics: The Clearwater River basin, Olympic Peninsula, Washington State. *Bulletin of the Geological Society of America*, *114*(6), 731–744. doi:10.1130/0016-7606(2002)114<0731:HSTCCA>2.0.CO;2

Westoby, M. J., Brasington, J., Glasser, N. F., Hambrey, M. J., & Reynolds, J. M. (2012). "Structure-from-Motion" photogrammetry: A low-cost, effective tool for geoscience applications. *Geomorphology*, *179*, 300–314. doi:10.1016/j.geomorph.2012.08.021

Whipple, K. X. (2004). Bedrock Rivers and the Geomorphology of Active Orogens. *Annual Review of Earth and Planetary Sciences*, *32*(1), 151–185. doi:10.1146/annurev.earth.32.101802.120356

Whipple, K. X., DiBiase, R. A., & Crosby, B. T. (2013). *Bedrock Rivers*. *Treatise on Geomorphology* (Vol. 9). Elsevier Ltd. doi:10.1016/B978-0-12-374739-6.00254-2

Whipple, K. X., Hancock, G. S., & Anderson, R. S. (2000). River incision into bedrock: Mechanics and relative efficacy of plucking, abrasion, and cavitation. *Bulletin of the*

Geological Society of America, *112*(3), 490–503. doi:10.1130/0016-7606(2000)112<490:RIIBMA>2.0.CO;2

Whipple, K. X., & Tucker, G. E. (1999). Dynamics of the stream-power river incision model: Implications for height limits of mountain ranges, landscape response timescales, and research needs. *Journal of Geophysical Research: Solid Earth*, *104*(B8), 17661–17674. doi:10.1029/1999JB900120

Whipple, K. X., & Tucker, G. E. (2002). Implications of sediment-flux-dependent river incision models for landscape evolution. *Journal of Geophysical Research*, *107*(B2). doi:10.1029/2000jb000044

Wickert, A. D., Martin, J. M., Tal, M., Kim, W., Sheets, B., & Paola, C. (2013). River channel lateral mobility: Metrics, time scales, and controls. *Journal of Geophysical Research: Earth Surface*, *118*(2), 396–412. doi:10.1029/2012JF002386

Wintle, A. G., & Murray, A. S. (2006). A review of quartz optically stimulated luminescence characteristics and their relevance in single-aliquot regeneration dating protocols. *Radiation Measurements*, *41*(4), 369–391. doi:10.1016/j.radmeas.2005.11.001

Wohl, E. E., & Ikeda, H. (1998). Patterns of Bedrock Channel Erosion on the Boso Peninsula, Japan. *The Journal of Geology*, *106*(3), 331–346. doi:10.1086/516026

Appendix A – Trail Camera Photos

Below are a few photographs from the trail cameras of high flow events during the summer and various erosion processes.

Figure A1 Example of mass block failure of limestone bedrock from the channel bank at the North Fork downstream site (red circle). The bottom image was captured 15 minutes after the top image.

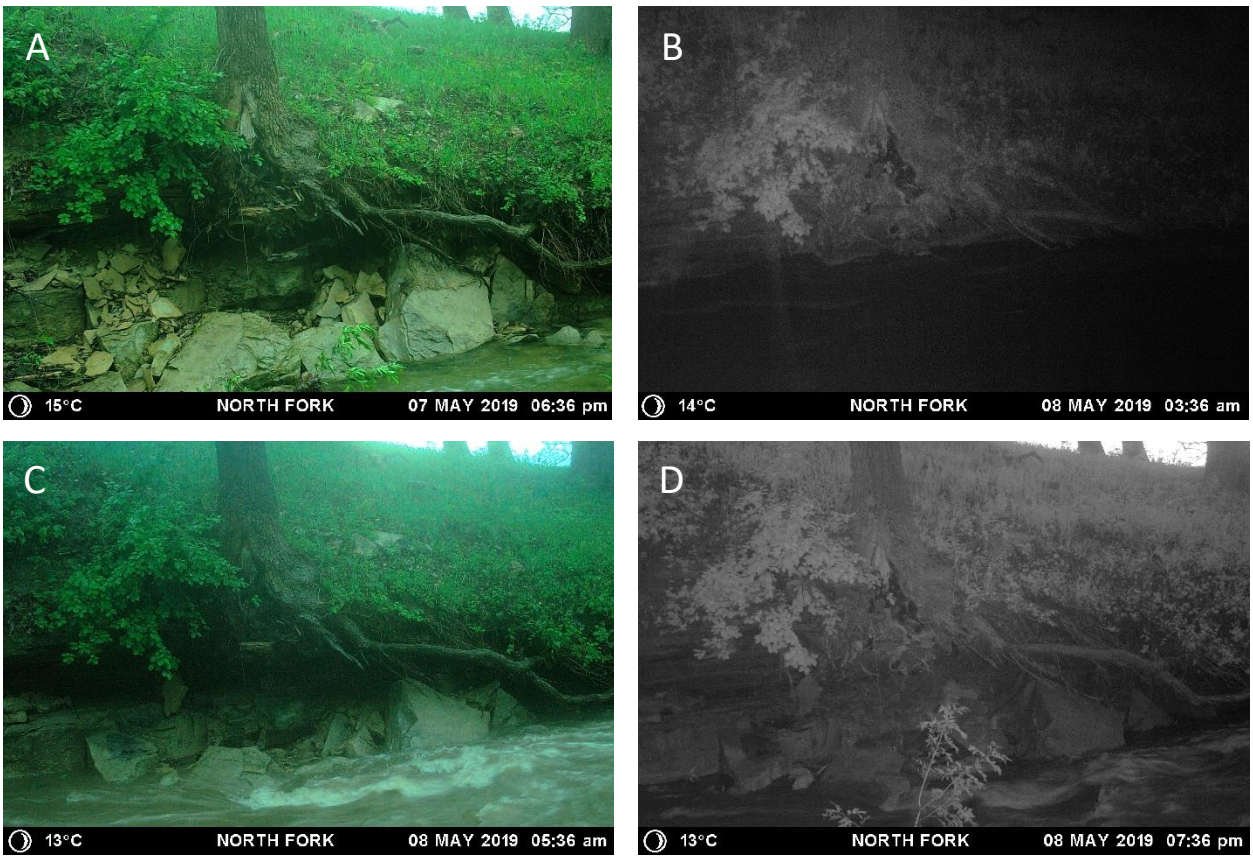

Figure A2 Example of a high flow event at the downstream North Fork site on May 7 & 8, 2019. Discharge data from USGS stream gauge #06879650 located downstream near the Nature Trail site. Measured peak flow for this event was 42.48 m^3/s. Discharge values are divided in half, given that the North Fork contributing drainage area is roughly half of the Nature Trail site's contributing drainage area. (A) Before the precipitation; (B) During the storm – stream discharge ~8.76 m^3/s (measured 17.52 m^3/s); (C) Stream discharge ~8.6 m^3/s (measured 17.2 m^3/s); (D) Stream discharge in this image is ~2.135 m^3/s (measured 4.27 m^3/s)

Figure A3 Evidence of plucking (red circles) at the downstream North Fork Site not present in the May 2019 trail camera images.

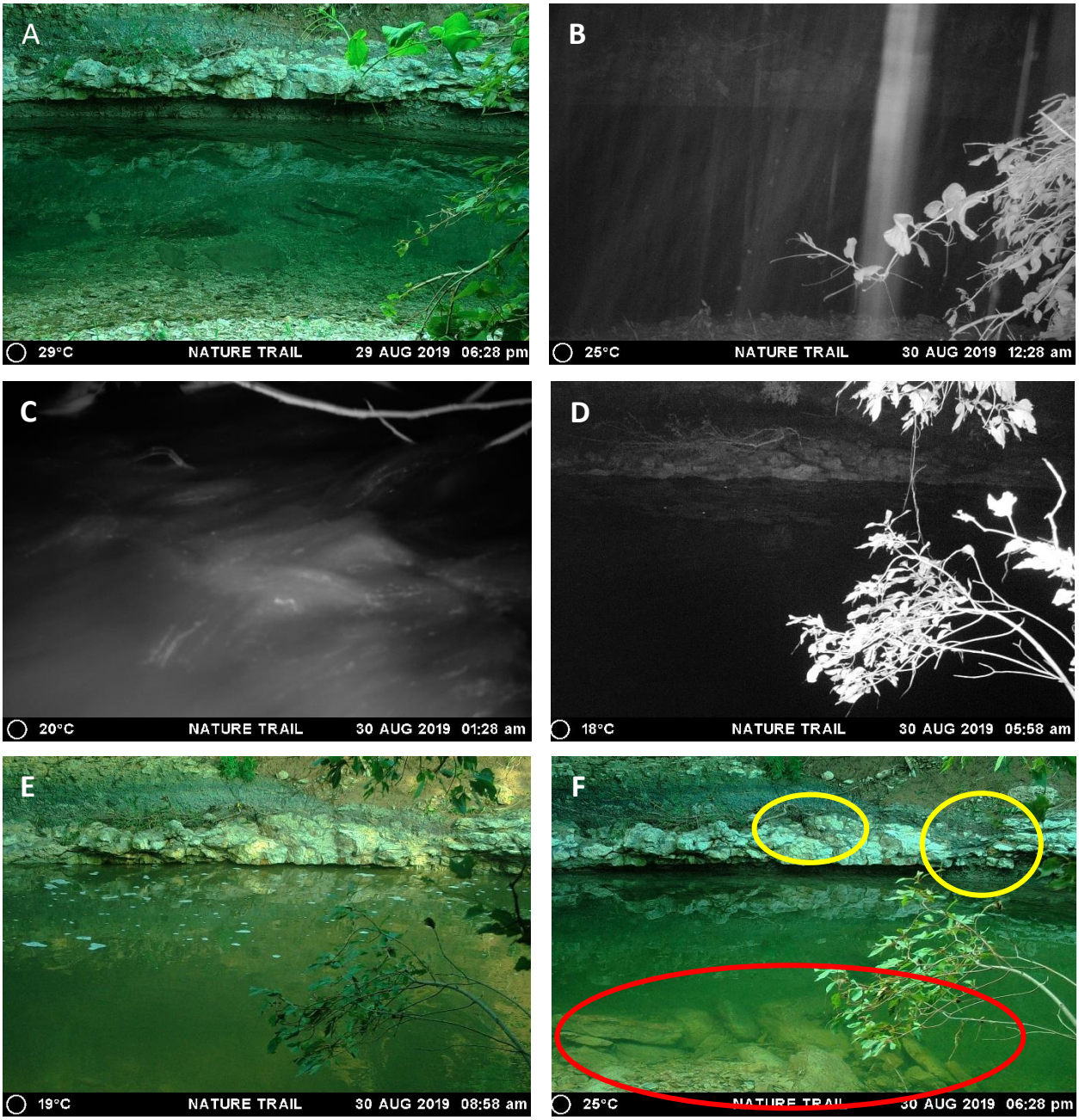

Figure A4 Example of a high flow event at the Nature Trail site on August 29 &30, 2019. Discharge data from USGS stream gauge #06879650 ~100 m upstream of the Nature Trail site. Measured peak flow for this event was 121.19 m^3/s at 01:38. (A) Before the precipitation; (C) Discharge is 79.57 m^3/s, just 10 minutes prior to peak flow; (D) Kings Creek water stage going down. Discharge is 2.06 m^3/s; (E) The water stage continues to lower. Discharge is 0.79 m^3/s; (F) Photo taken 24 hours after photo A. Kings Creek transported several large boulders (red circle) during the flow event and removed limestone blocks from the channel bank (yellow circles).